Linear Waves at Viscoelastic Interfaces Between Viscoelastic Media

Sina Zendehroud,[1] Roland R. Netz,[1] and Julian Kappler[1,2]

[1] *Freie Universität Berlin, Department of Physics, Arnimallee 14, 14195 Berlin, Germany*
[2] *University of Cambridge, Wilberforce Road, DAMTP, Centre for Mathematical Sciences, Cambridge CB3 0WA, United Kingdom*

(Dated: May 6, 2021)

We derive the general dispersion relation for interfacial waves along a planar viscoelastic boundary that separates two viscoelastic bulk media, including the effect of gravity. Our unified theory contains Rayleigh waves, capillary-gravity-flexural waves, Lucassen waves, bending waves in elastic plates, and the standard dispersion-free sound waves, as limiting cases. To illustrate our results, we consider waves at a viscoelastic interface immersed in water, and also at an air-water interface. We furthermore investigate pressure waves at a viscoelastic interface separating two identical viscoelastic bulk media, for which we consider both Kelvin-Voigt and Maxwell materials, as applicable to polymer gels and solutions. For all cases, we study how material properties determine the crossovers, scaling, and existence regimes, of the various interfacial waves. Since we include viscoelastic effects for all media involved, our theory allows to model waveguiding phenomena in biology, such as pressure pulses in axon membranes, which are possibly relevant for acoustic nerve pulse propagation phenomena.

I. INTRODUCTION

Waves at interfaces are well-known and can be observed in everyday life. A classical example is the capillary-gravity wave on an incompressible Newtonian fluid under the influence of gravity [1–6]. The theory of this wave has been extended to include both interfacial properties such as bending rigidity [7], and to include viscoelastic shear response in the bulk, as applicable to e.g. gels [8]. If the interface responds viscoelastically to compression, then a second type of surface wave can coexist with the capillary-gravity wave. We refer to this interfacial pressure wave as Lucassen wave [9–12]; it has recently received attention because of its possible relevance for acoustic nerve pulse propagation [13–16]. For elastic materials where the interfacial properties are negligible, a third kind of surface wave exists, which is called the Rayleigh wave [17]. If the material is viscoelastic, two such waves can coexist [18, 19]. Viscoelastic Rayleigh waves are of particular interest e.g. in geophysics, as a model for earthquake-generated waves [20], or in material engineering, to measure mechanical properties of media non-invasively [21]. If gravitation, surface tension and bulk shear viscosity are simultaneously nonzero, capillary-gravity-viscous (CGV) surface waves can exist, which are different from all the above waves, and have only very recently been discovered [22].

Localized waves at fluid interfaces have recently gained renewed attention in the search of a more complete picture of nerve pulse propagation [23–29]. While the standard Hodgkin-Huxley model is successful in modeling the observed electrical phenomena, it does not account for several other aspects of nerve pulse propagation. Examples are the Meyer-Overton rule, which states that the effectiveness of an anaesthetic is directly proportional to its solubility in a lipid membrane [30, 31], and that the net heat release of an axon during a nerve pulse is less than expected from the Ohmic heating of an electrical cable [32]. In particular, it is known that a mechanical displacement propagates alongside the electrical pulse [33, 34].

For the modeling of biologically relevant surface wave phenomena, a natural theoretical model is given by a viscoelastic interface separating two viscoelastic media. In the biological setting, e.g. when comparing the axoplasm to the extracellular fluid separated by an axon membrane, the bulk media on both sides will rarely differ so much as to justify neglecting one of them. Hydrodynamic modes of a thin viscoelastic material at the interface between two Newtonian fluids where already discussed in Ref. [35]. The dynamics of viscoelastic membranes separating two Newtonian fluids have been studied with regard to microrheological studies of such membranes [36]. Recently, a comprehensive dispersion relation has been derived for linear waves at a surfactant layer separating two Newtonian fluids, supporting capillary-gravity waves and Lucassen waves as solutions [37, 38]. However, the general case of two viscoelastic media separated by a viscoelastic interface has not been considered before.

For a viscoelastic half-space, which is an appropriate model if one of the bulk media is negligible, recently a general surface wave dispersion relation was derived, which contained Rayleigh, capillary-gravity, and Lucassen waves as limiting cases [22]. This allowed to discuss the relation between those waves: For water, modeled as an almost incompressible viscoelastic medium, the Lucassen wave transforms into a Rayleigh wave at high frequencies. Waves on half-spaces of a viscoelastic solid were investigated numerically in order to model rheological applications in Refs. [39, 40], while capillary waves on viscoelastic half-spaces have been studied numerically in Refs. [41, 42].

If the media at the two sides of an elastic interface can be neglected, then transversal oscillations of the interface are described by elastic plate theory [43], while compression waves within the interface are described by

a standard wave equation.

For capillary-gravity waves, the relation between the model of two fluid half-spaces and the model of just one fluid half-space has been explored [37], but generally the relation between the theories for interfacial waves with two fluid half-spaces, one fluid half-space, and an oscillating plate in vacuum, has not been discussed.

In the present work, we derive the general dispersion relation for waves at planar viscoelastic interfaces separating two different linear isotropic homogeneous viscoelastic half-spaces including the effects of gravity. We show how the interfacial capillary-gravity and Lucassen waves follow from a factorization of the general dispersion relation. After considering the symmetric case, where the two bulk media have the same properties, we then first discuss the limit where one of the bulk media is negligible, and second the limit where both bulk media can be neglected. Our derivation shows explicitly that the elastic plate equation can be considered as a limit of the capillary-gravity-flexural wave, i.e. the capillary-gravity wave for an interface with bending rigidity. The one-dimensional wave equation, in turn, is recovered as a limit of the Lucassen wave.

We go on to discuss several explicit scenarios. We consider localized waves at a water-water interface, and at an air-water interface (where we show that the half-space of air can be neglected). We then consider the case of an interface separating two viscoelastic bulk media, modeled via Kelvin-Voigt and Maxwell materials, respectively. For every explicit scenario, we highlight the different power-law scalings of phase velocities and propagation distances emerging from the model. We finally discuss how the properties of pressure waves at viscoelastic interfaces are consistent with both the effect of myelin on nerve pulse propagation, as well as with the Meyer-Overton rule, as has been noted before [23].

The organization of this paper is as follows: In Sec. II, we establish the framework of our calculations and derive a general dispersion relation for our setup: In Sec. II A, we review linear viscoelasticity and explain how the viscoelastic properties of the interface enter the theory in the form of boundary conditions. In Sec. II B, we demonstrate how, for our setup, the harmonic wave ansatz leads to a conditional equation whose solutions describe traveling waves localized at the interface. In Sec. II C, we show that the conditional equation factorizes under appropriate conditions, leading to generalized approximate dispersion relations for capillary-gravity waves and longitudinal capillary waves. In Sec. III, we discuss how special cases known from the literature arise in various limits, namely the symmetric case, where media I, III are equal, the situation where medium III is absent, here called asymmetric case, and waves on a free membrane. In Sec. IV, after a review of viscoelastic relaxation functions for Newtonian fluids, we then consider numerical solutions of both the general dispersion relation and the appropriate limits, focusing on waves at the water-water interface and on waves at the air-water interface, showing that air is mostly negligible when paired with water. We investigate interfaces of viscoelastic bulk media, specifically polymer gels, modeled as Kelvin-Voigt materials, and concentrated polymer solutions, modeled as Maxwell-fluids. For all example systems, we discuss the different power-law scalings and crossovers in detail. Finally, in Sec. V we summarize our findings and discuss implications as well as applications.

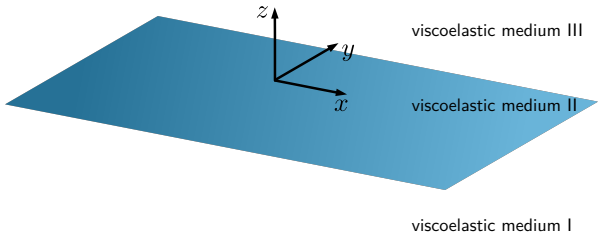

FIG. 1. In this work, we consider a planar viscoelastic interface (medium II), which is located at $z = 0$ and separates two viscoelastic bulk media (media I and III), which are infinitely extended in the half-spaces $z < 0$, $z > 0$. All viscoelastic media are modeled as linear, isotropic, homogeneous. We include gravitational acceleration, which acts in the negative z-direction. We consider wave solutions which travel in the positive x-direction, are translationally invariant in the y-direction, and decay exponentially away from the interface at $z = 0$.

Because there is a great variety of notations in hydrodynamics and viscoelasticity theory, we have compiled a list of all material parameters appearing in this paper in Appendix A.

II. GENERAL DISPERSION RELATION FOR WAVES AT VISCOELASTIC INTERFACES

We study localized waves at a viscoelastic interface between two viscoelastic media, as illustrated in Fig. 1. We choose the coordinate system such that the interface is at $z = 0$, and refer to the bulk media in the lower and upper half-spaces as medium I and medium III, respectively. The interface itself we call medium II. We assume all displacements to be small, and use the linear theory of viscoelasticity for the description of media I and III. Medium II enters the dynamics via the boundary conditions at the interface.

The following derivation is a generalization of Ref. [22] and follows the standard derivation of Rayleigh waves [17].

A. Linear Viscoelasticity

In each of the two bulk media, the linearized equations for momentum conservation are given at a position $\boldsymbol{r} =$

(x, y, z) and time t as [44]

$$\rho_M(\boldsymbol{r},t)\partial_t^2 u_{M,j}(\boldsymbol{r},t) = \partial_k \sigma_{M,jk}(\boldsymbol{r},t) + F_j(\boldsymbol{r},t) \tag{1}$$

for $j \in \{x,y,z\}$, where $M \in \{\mathrm{I},\mathrm{III}\}$ denotes the bulk medium, so that for $z<0$ we have $M=\mathrm{I}$ and for $z>0$ we have $M=\mathrm{III}$, $\rho_M(\boldsymbol{r},t)$ is the respective mass density, $\boldsymbol{u}_M(\boldsymbol{r},t)$ is the displacement field, $\boldsymbol{F}(\boldsymbol{r},t)$ is an external force, and where we use the Einstein summation convention for repeated indices. We assume linear, isotropic, and homogeneous bulk media, for which the stress tensor components $\sigma_{M,jk}(\boldsymbol{r},t)$ depend on the displacement via the viscoelastic stress-strain relation [44]

$$\begin{aligned}\sigma_{M,jk}(\boldsymbol{r},t) = &\int_{-\infty}^{\infty} g_{M,s}(t-t')\partial_{t'}\epsilon_{M,jk}(\boldsymbol{r},t')\,\mathrm{d}t' \\ &+ \frac{\delta_{jk}}{3}\int_{-\infty}^{\infty}\left[g_{M,d}(t-t') - g_{M,s}(t-t')\right]\partial_{t'}\epsilon_{M,ll}(\boldsymbol{r},t')\,\mathrm{d}t' \ ,\end{aligned} \tag{2}$$

where the components of the strain tensor are given by $\epsilon_{M,jk} = \left(\partial_j u_{M,k} + \partial_k u_{M,j}\right)/2$, and by the Einstein summation convention we have $\epsilon_{M,ll} = \partial_l u_{M,l} = \boldsymbol{\nabla}\cdot\boldsymbol{u}_M$. For homogeneous media, the shear and dilational relaxation functions $g_{M,s}(t)$, $g_{M,d}(t)$ are independent of position, and to ensure causality are equal to zero for negative arguments t.

For the interface, medium II, we assume a purely viscous shear response with viscosity $\eta_{2\mathrm{D}}$, a viscoelastic response under dilation with viscosity $\eta'_{2\mathrm{D}}$, and a position-dependent surface tension σ. For out of plane deformations, we consider a bending rigidity κ_{2D} and a transverse viscosity $\eta^{\perp}_{2\mathrm{D}}$. Furthermore, the interface has an excess area mass density $\rho_{2\mathrm{D}}$. A review for the derivation of the continuum-mechanical boundary conditions of two bulk media divided by such a viscoelastic interface was given by Kralchevsky et. al. [45]; the resulting linearized stress-continuity condition for the displacement field at $z=0$ has been derived in Ref. [22], and is reproduced in App. B. Further below, we use this continuity condition to relate the two solutions $\boldsymbol{u}_{\mathrm{I}}(\boldsymbol{r},t)$, $\boldsymbol{u}_{\mathrm{III}}(\boldsymbol{r},t)$ at the interface $z=0$.

We consider gravity as external force, $\boldsymbol{F}(\boldsymbol{r},t) = -g\hat{e}_z$, where $g = 9.81\,\mathrm{m/s^2}$ is the gravitational acceleration and $\hat{e}_z$ is the unit vector pointing in the positive z-direction. We use the surface gravity approximation [46], for which the effect of gravity on media I, II, and III, only enters at the boundary condition $z=0$ and not in the equations of motion of the bulk media; for more details see Ref. [22].

B. Harmonic Wave Ansatz and Resulting Dispersion Relation

To solve the momentum conservation equations Eq. (1) for bulk medium M, we describe the displacement fields $\boldsymbol{u}_M(\boldsymbol{r},t)$ via displacement potentials $\varphi_M(\boldsymbol{r},t)$, $\boldsymbol{\psi}_M(\boldsymbol{r},t)$ as

$$\boldsymbol{u}_M = \boldsymbol{\nabla}\varphi_M + \boldsymbol{\nabla}\times\boldsymbol{\psi}_M \ . \tag{3}$$

If the temporal Fourier transforms of the displacement potentials satisfy the Helmholtz equations

$$\rho_M(-i\omega)\tilde{\varphi}_M = \frac{1}{3}\left(2\tilde{g}_{M,s} + \tilde{g}_{M,d}\right)\Delta\tilde{\varphi}_M \tag{4}$$

$$\rho_M(-i\omega)\tilde{\psi}_{M,j} = \frac{1}{2}\tilde{g}_{M,s}\Delta\tilde{\psi}_{M,j} \ , \qquad \text{for } j\in\{x,y,z\} \ , \tag{5}$$

where $\Delta = \partial_x^2 + \partial_y^2 + \partial_z^2$ is the Laplace operator and the tilde signifies the temporal Fourier transform, then the displacement fields (3) fulfill the linearized momentum conservation equation (1) for a linear, isotropic, homogeneous viscoelastic material with stress-strain relation (2) and without external forces, as appropriate for the surface gravity approximation. The densities ρ_M in Eqs. (4), (5) denote the constant equilibrium densities of the steady state solution, around which we perturb [22]. To obtain a stable equilibrium around which the linear wave solutions are derived by perturbation, we assume that $\rho_{\mathrm{I}} \geq \rho_{\mathrm{III}}$, i.e. that the less dense medium is always in the $z>0$ half-space.

The harmonic wave ansatz [17] consists of choosing the displacement potentials

$$\varphi_M(x,z,t) = \Phi_M \exp\left(-\lambda_{M,l}^{-1}|z|\right)\exp\left[i\left(kx-\omega t\right)\right] \ , \tag{6}$$

$$\psi_{M,j}(x,z,t) = \Psi_M \exp\left(-\lambda_{M,t}^{-1}|z|\right)\exp\left[i\left(kx-\omega t\right)\right]\delta_{jy} \ , \tag{7}$$

where $j\in\{x,y,z\}$, $M\in\{\mathrm{I},\mathrm{III}\}$, and we assume the angular frequency $\omega\in\mathbb{R}$ is a given parameter, while the wave number k, the decay lengths $\lambda_{M,l}$, $\lambda_{M,t}$, and the coefficients Φ_M, $\Psi_M\in\mathbb{C}$ depend on ω. For $M=\mathrm{I}$ we have $z<0$, and for $M=\mathrm{III}$ we have $z>0$, so that the requirement that the displacement decays to zero as $|z|\to\infty$ implies $\mathrm{Re}(\lambda_{M,l}^{-1})$, $\mathrm{Re}(\lambda_{M,t}^{-1})>0$. Our choice $\omega\in\mathbb{R}$, $k\in\mathbb{C}$ means we consider plane wave solutions with frequency ω, which are damped as they propagate along the x-axis, and that we will later solve for $k(\omega)$.

Direct substitution shows that in each half-space, the harmonic wave ansatz fulfills Eqs. (4), (5) if [22]

$$\lambda_{M,l}^{-2}(k,\omega) = k^2 + \gamma_M^2(\omega) \tag{8}$$

$$\lambda_{M,t}^{-2}(k,\omega) = k^2 + \alpha_M^2(\omega) \ , \tag{9}$$

where we define

$$\gamma_M^2(\omega) := \frac{3(-i\omega)\rho_M}{2\tilde{g}_{M,s}(\omega) + \tilde{g}_{M,d}(\omega)} \tag{10}$$

$$\alpha_M^2(\omega) := \frac{2(-i\omega)\rho_M}{\tilde{g}_{M,s}(\omega)} \ . \tag{11}$$

Equations (8), (9) and the requirement $\mathrm{Re}(\lambda_{M,l}^{-1})$, $\mathrm{Re}(\lambda_{M,t}^{-1})>0$ determine $\lambda_{M,l}^{-1}, \lambda_{M,t}^{-1}$ uniquely [47].

For a given frequency ω, the harmonic wave ansatz then contains five unknowns, namely k, Φ_{I}, Ψ_{I}, Φ_{III}, Ψ_{III}.

Continuity of the two non-vanishing components of the displacement field at $z = 0$, and the stress boundary conditions at $z = 0$, yield a homogeneous linear system of four equations for the four coefficients Φ_{I}, Ψ_{I}, Φ_{III} and Ψ_{III}, which is given explicitly in App. B. For a propagating wave with nonzero amplitude, this linear system of equations needs to have a nontrivial solution, which means that the determinant of the coefficient matrix vanishes. Equating this determinant with zero then gives rise to the general dispersion relation

$$
\begin{aligned}
0 = {} & 4\left(k^2\tilde{\Pi}_{2\mathrm{D}} + g(\rho_{\mathrm{I}} - \rho_{\mathrm{III}}) - \omega^2\rho_{2\mathrm{D}}\right) \\
& \times \left[(k^2\tilde{g}_{2\mathrm{D}} - i\omega\rho_{2\mathrm{D}})(k^2 - \lambda_{\mathrm{I},l}^{-1}\lambda_{\mathrm{I},t}^{-1})(k^2 - \lambda_{\mathrm{III},l}^{-1}\lambda_{\mathrm{III},t}^{-1}) + i\omega\rho_{\mathrm{I}}\lambda_{\mathrm{I},l}^{-1}(k^2 - \lambda_{\mathrm{III},l}^{-1}\lambda_{\mathrm{III},t}^{-1}) + i\omega\rho_{\mathrm{III}}\lambda_{\mathrm{III},l}^{-1}(k^2 - \lambda_{\mathrm{I},l}^{-1}\lambda_{\mathrm{I},t}^{-1}) \right] \\
& + 4(k^2\tilde{g}_{2\mathrm{D}} - i\omega\rho_{2\mathrm{D}})\omega^2 \left[\rho_{\mathrm{I}}\lambda_{\mathrm{I},t}^{-1}(k^2 - \lambda_{\mathrm{III},l}^{-1}\lambda_{\mathrm{III},t}^{-1}) + \rho_{\mathrm{III}}\lambda_{\mathrm{III},t}^{-1}(k^2 - \lambda_{\mathrm{I},l}^{-1}\lambda_{\mathrm{I},t}^{-1}) \right] \\
& + \tilde{g}_{\mathrm{I},s}(k^2 - \lambda_{\mathrm{III},l}^{-1}\lambda_{\mathrm{III},t}^{-1}) \left[i\omega\tilde{g}_{\mathrm{I},s}\left(-4k^2\lambda_{\mathrm{I},l}^{-1}\lambda_{\mathrm{I},t}^{-1} + (k^2 + \lambda_{\mathrm{I},t}^{-2})^2\right) + 2\rho_{2\mathrm{D}}gk^2\left(2\lambda_{\mathrm{I},l}^{-1}\lambda_{\mathrm{I},t}^{-1} - (k^2 + \lambda_{\mathrm{I},t}^{-2})\right) \right] \\
& + \tilde{g}_{\mathrm{III},s}(k^2 - \lambda_{\mathrm{I},l}^{-1}\lambda_{\mathrm{I},t}^{-1}) \left[i\omega\tilde{g}_{\mathrm{III},s}\left(-4k^2\lambda_{\mathrm{III},l}^{-1}\lambda_{\mathrm{III},t}^{-1} + (k^2 + \lambda_{\mathrm{III},t}^{-2})^2\right) - 2\rho_{2\mathrm{D}}gk^2\left(2\lambda_{\mathrm{III},l}^{-1}\lambda_{\mathrm{III},t}^{-1} - (k^2 + \lambda_{\mathrm{III},t}^{-2})\right) \right] \\
& + (-i\omega)\tilde{g}_{\mathrm{I},s}\tilde{g}_{\mathrm{III},s} \Big[2k^2(k^2 + \lambda_{\mathrm{I},t}^{-2})(k^2 + \lambda_{\mathrm{III},t}^{-2}) + \alpha_{\mathrm{I}}^2\alpha_{\mathrm{III}}^2(\lambda_{\mathrm{I},t}^{-1}\lambda_{\mathrm{III},l}^{-1} + \lambda_{\mathrm{III},t}^{-1}\lambda_{\mathrm{I},l}^{-1}) \\
& \quad + 8k^2\lambda_{\mathrm{I},l}^{-1}\lambda_{\mathrm{I},t}^{-1}\lambda_{\mathrm{III},l}^{-1}\lambda_{\mathrm{III},t}^{-1} - 4k^2\lambda_{\mathrm{I},l}^{-1}\lambda_{\mathrm{I},t}^{-1}(k^2 + \lambda_{\mathrm{III},t}^{-2}) - 4k^2\lambda_{\mathrm{III},l}^{-1}\lambda_{\mathrm{III},t}^{-1}(k^2 + \lambda_{\mathrm{I},t}^{-2}) \Big] \ , \qquad (12)
\end{aligned}
$$

where we introduced the in-plane membrane relaxation function

$$(-i\omega)\tilde{g}_{2\mathrm{D}}(\omega) := (-i\omega)(\eta_{2\mathrm{D}} + \eta'_{2\mathrm{D}}) + K_{2\mathrm{D}} \qquad (13)$$

and the out-of-plane membrane relaxation function

$$\tilde{\Pi}_{2\mathrm{D}}(k,\omega) := (-i\omega)\eta_{2\mathrm{D}}^{\perp} + \sigma_{2\mathrm{D}} + k^2\kappa_{2\mathrm{D}} \ . \qquad (14)$$

Because $\eta_{2\mathrm{D}}$ and $\eta'_{2\mathrm{D}}$ only appear summed together, in Eq. (13), we in the following set $\eta'_{2\mathrm{D}} = 0$, with the understanding that $\eta_{2\mathrm{D}}$ includes the effects of both interfacial shear and dilational viscosity.

The above Eq. (12) describes general surface waves at the viscoelastic interface between two viscoelastic bulk fluids, and is the main result of this paper. If the effect of gravity is removed, $g = 0$, then the equation becomes symmetric under the interchange of the indices $\mathrm{I} \leftrightarrow \mathrm{III}$.

A solution $k(\omega)$ of Eq. (12) represents a surface wave solution; the corresponding phase velocity $c(\omega)$ and propagation distance $\beta^{-1}(\omega)$ are given by

$$c(\omega) = \frac{\omega}{\mathrm{Re}\left(k(\omega)\right)}, \qquad (15)$$

$$\beta^{-1}(\omega) = \frac{1}{\mathrm{Im}\left(k(\omega)\right)}. \qquad (16)$$

For decaying plane wave solutions that travel in the positive x-direction, we are therefore interested in solutions $k(\omega)$ with $\mathrm{Re}(k(\omega)), \mathrm{Im}(k(\omega)) > 0$. For later reference we note that from Eqs. (15), (16) it follows that if

$$k \sim \omega^{\nu} \qquad (17)$$

for some real number ν, then

$$c \sim \omega^{1-\nu}, \qquad \beta^{-1} \sim \omega^{-\nu}. \qquad (18)$$

As it stands, Eq. (12) is too complicated to allow for general analytic solutions. However, as we discuss in the following sections, and as has been noted for special cases before [8, 35, 48, 49], many known surface wave types can be retrieved from this equation in suitable limits.

C. Factorization of the Dispersion Relation

If for both bulk media the condition [22]

$$\frac{3\omega\rho_M}{|2\tilde{g}_{M,s}(\omega) + \tilde{g}_{M,d}(\omega)|} \ll |k^2(\omega)| \ll \frac{2\omega\rho_M}{|\tilde{g}_{M,s}(\omega)|} \qquad (19)$$

holds for $M \in \{\mathrm{I}, \mathrm{III}\}$, and additionally assuming that the gravitational force on the interface can be neglected, i.e.

$$\rho_{2\mathrm{D}}g \ll \omega|\tilde{g}_{M,s}(\omega)| \ , \qquad M \in \{\mathrm{I}, \mathrm{III}\} \ , \qquad (20)$$

then Eq. (12) factorizes to

$$
\begin{aligned}
0 = {} & \left[k^2\tilde{\Pi}_{2\mathrm{D}} + g(\rho_{\mathrm{I}} - \rho_{\mathrm{III}}) - \omega^2(\rho_{2\mathrm{D}} + \rho_{\mathrm{I}}\lambda_{\mathrm{I},l} + \rho_{\mathrm{III}}\lambda_{\mathrm{III},l})\right] \\
& \times \left[k^2\tilde{g}_{2\mathrm{D}} - i\omega\left(\rho_{2\mathrm{D}} + \rho_{\mathrm{I}}\lambda_{\mathrm{I},t} + \rho_{\mathrm{III}}\lambda_{\mathrm{III},t}\right)\right] . \qquad (21)
\end{aligned}
$$

By equating either of the two factors with zero, we obtain two independent dispersion relations. Whether a

solution $k(\omega)$ of either of the resulting equations fulfills the factorization conditions Eqs. (19), (20), can of course only be checked *a posteriori*.

According to Eqs. (8), (9), in the limit Eq. (19) we obtain

$$\lambda_{M,t}^{-2} \approx \alpha_M^2, \qquad \lambda_{M,l}^{-2} \approx k^2 \ . \tag{22}$$

Both inequalities in Eq. (19) can be interpreted physically. According to Eqs. (3), (6), (8), the left inequality implies that $\lambda_{M,l}^{-2} \approx k^2$, so that $\boldsymbol{\nabla} \cdot \boldsymbol{u}_M \approx 0$, which means that the medium is almost incompressible. The right inequality in Eq. (19), on the other hand, can be interpreted physically as a long-wavelength limit. The inequality implies that $\lambda_{M,t}^{-2} \approx \alpha^2$ in Eq. (22), which according to Eqs. (7), (9) means that the decay length of the transversal potential $\boldsymbol{\psi}_M$ away from the interface $z = 0$ is much smaller than the modulus of the inverse wave number, $1/|k|$, with which the wave propagates along the interface, i.e. $1/|k| \gg |\lambda_{M,t}|$.

The first factor in Eq. (21) yields a generalization of the dispersion relation for capillary-gravity waves on a viscoelastic interface between two unbounded fluids, and can be rearranged as

$$\tilde{\Pi}_{2\mathrm{D}} k^2 + (\rho_{\mathrm{I}} - \rho_{\mathrm{III}}) g = \omega^2 \left(\rho_{2\mathrm{D}} + \rho_{\mathrm{I}} \lambda_{\mathrm{I},l} + \rho_{\mathrm{III}} \lambda_{\mathrm{III},l}\right) , \tag{23}$$

where $\tilde{\Pi}_{2\mathrm{D}}$ is given by Eq. (14). Assuming the bending rigidity in $\tilde{\Pi}_{2\mathrm{D}}$ is negligible, a crossover from surface-tension driven waves to a transverse-viscosity dominated response occurs at the frequency

$$\omega_{2\mathrm{D}}^{\sigma} \equiv \frac{\sigma_{2\mathrm{D}}}{\eta_{2\mathrm{D}}^{\perp}} \ . \tag{24}$$

We give a physical interpretation of Eq. (23) by observing that the equation formally looks similar to a Fourier transformed wave equation with additional restoring force. This becomes more obvious upon rewriting the equation as

$$\tilde{\Pi}_{2\mathrm{D}} (ik)^2 - (\rho_{\mathrm{I}} - \rho_{\mathrm{III}}) g = (-i\omega)^2 \left(\rho_{2\mathrm{D}} + \rho_{\mathrm{I}} \lambda_{\mathrm{I},l} + \rho_{\mathrm{III}} \lambda_{\mathrm{III},l}\right) . \tag{25}$$

The right-hand side contains a factor $(-i\omega)^2$, which represents a second temporal derivative and hence describes an acceleration. The effective area mass density which couples to this inertia is given by the sum of the excess area mass density $\rho_{2\mathrm{D}}$ and the effective area mass densities associated with the longitudinal part of the wave. To see this, we note that according to Eq. (6), $\lambda_{M,l}$ represents the penetration depth of the longitudinal part of the wave into bulk medium M, so that $\rho_M \lambda_{M,l}$ is the effective area mass density of the longitudinal oscillation in medium M. That the longitudinal part of the displacement is dominant for capillary-gravity-flexural waves is plausible, as for inviscid incompressible Euler flow the capillary-gravity dispersion relation can be derived assuming only a longitudinal displacement field [3]. The inertia term in Eq. (25) is balanced by a linear restoring force, with strength $(\rho_{\mathrm{I}} - \rho_{\mathrm{III}})g$, and a force coupling to the surface deformation, represented by $\tilde{\Pi}_{2\mathrm{D}}(ik)^2$. According to Eq. (14), this force has elastic, dissipative, and bending, components. Performing an inverse Fourier transform of Eq. (25) is not straightforward, for two reasons. First, $\lambda_{M,l}$ depends on both k and ω via a complex square root, so that it in general does not correspond to a simple spatial or temporal derivative in real space. Second, since we here derive the dispersion relation via the harmonic wave ansatz, the physical interpretation of the function that obeys the inverse-Fourier-transformed Eq. (25) is not obvious. From comparing the dispersion relation Eq. (25) with the stress tensor boundary conditions for the surface displacement in the z-direction, which is given in App. B, it is plausible that Eq. (25) is the Fourier transformed equation of motion for the surface displacement in the z-direction; however, showing this rigorously is beyond the scope of the current work.

The second factor in Eq. (21) corresponds to a generalization of the Lucassen dispersion relation [10, 12], and results in

$$k^2 = \frac{i\omega}{\tilde{g}_{2\mathrm{D}}} (\rho_{2\mathrm{D}} + \rho_{\mathrm{I}} \lambda_{\mathrm{I},t} + \rho_{\mathrm{III}} \lambda_{\mathrm{III},t}) \ , \tag{26}$$

where $\tilde{g}_{2\mathrm{D}}$ is defined in Eq. (13). This equation also has a physical interpretation in terms of a force balance equation [16]. To see this, we first rewrite the dispersion relation as

$$-i\omega (ik)^2 \tilde{g}_{2\mathrm{D}} = (-i\omega)^2 (\rho_{2\mathrm{D}} + \rho_{\mathrm{I}} \lambda_{\mathrm{I},t} + \rho_{\mathrm{III}} \lambda_{\mathrm{III},t}) \ . \tag{27}$$

For a half-space filled with an incompressible Newtonian fluid, and bounded by a purely elastic membrane, it has been shown that Eq. (27) describes the interfacial displacement in the x-direction, so that the equation describes a compression wave. Furthermore, for the Newtonian-fluid model the inverse Fourier transform has been carried out explicitly, to derive a fractional wave equation [16]. We here recall the interpretation of Eq. (27) as equation of motion for the in-plane interface displacement: The right-hand side has a factor $(-i\omega)^2$, and hence corresponds to the acceleration of the interface. The effective area mass density relevant for this inertia term consists of three contributions, namely the excess interface area mass density $\rho_{2\mathrm{D}}$, and the effective area mass density of the bulk media oscillating above and below the interface, which for the Lucassen wave is dominated by the transversal motion and hence given by $\rho_{\mathrm{I}} \lambda_{\mathrm{I},t}$ and $\rho_{\mathrm{III}} \lambda_{\mathrm{III},t}$. The penetration depth of the wave into the bulk medium, $\lambda_{M,t}$, in general depends on the angular frequency ω, so that the effective area mass density becomes frequency-dependent. Because of this, it is not possible to explicitly perform the inverse Fourier transform of Eq. (27) without specifying the viscoelastic response of the bulk media. The left-hand side of Eq. (27) describes the force with which the interface responds to local compression along the interface, as described by the factor $(ik)^2$. Using Eq. (13) the prefactor

becomes $-i\omega\tilde{g}_{2\mathrm{D}}(\omega) = (-i\omega)\eta_{2\mathrm{D}} + K_{2\mathrm{D}}$, so that local compression of the interface leads to both an elastic response, described by $K_{2\mathrm{D}}$, and dissipation, described by $\eta_{2\mathrm{D}}$.

The generalized Lucassen dispersion relation Eq. (27) gives rise to several crossover frequencies. Whether for a given frequency the inertia term is dominated by the bulk media or the interface can be estimated by comparing $\rho_{2\mathrm{D}}$ with $\rho_{\mathrm{I}}|\lambda_{\mathrm{I},t}| + \rho_{\mathrm{III}}|\lambda_{\mathrm{III},t}|$. By equating these two expressions, and using $\lambda_{M,t}^{-1} \approx \alpha_M$ together with Eq. (11), we obtain the corresponding crossover frequency $\omega_{2\mathrm{D}}^{\rho}$ as solution of the equation

$$\frac{\sqrt{\rho_{\mathrm{I}}|\tilde{g}_{\mathrm{I},s}(\omega_{2\mathrm{D}}^{\rho})|} + \sqrt{\rho_{\mathrm{III}}|\tilde{g}_{\mathrm{III},s}(\omega_{2\mathrm{D}}^{\rho})|}}{\sqrt{2\omega_{2\mathrm{D}}^{\rho}}} = \rho_{2\mathrm{D}}. \tag{28}$$

If the expression on the left-hand side of this equation, when evaluated at an angular frequency ω, is much smaller than the expression on the right-hand side, inertia effects of the bulk media dominate over those of the interface, and vice versa. Similarly, whether the response of the membrane to compression is dominated by elasticity or viscosity switches at the crossover frequency

$$\omega_{2\mathrm{D}}^{\mathrm{elastic}} \equiv \frac{K_{2\mathrm{D}}}{\eta_{2\mathrm{D}}}. \tag{29}$$

For $\omega \ll \omega_{2\mathrm{D}}^{\mathrm{elastic}}$, the membrane response is predominantly elastic, whereas for $\omega \gg \omega_{2\mathrm{D}}^{\mathrm{elastic}}$, viscous dissipation dominates.

We remark that $\lambda_{M,l}$ and the bending properties $\kappa_{2\mathrm{D}}$ and $\eta_{2\mathrm{D}}^{\perp}$ (which are contained in $\tilde{\Pi}_{2\mathrm{D}}$) only enter the dispersion relation Eq. (23), while $\lambda_{M,t}$ and the in-plane viscoelastic response of the surface, described by $\eta_{2\mathrm{D}}$, $K_{2\mathrm{D}}$ (which are contained in $\tilde{g}_{2\mathrm{D}}$), only enter Eq. (26). This is consistent with the picture of the capillary-gravity-flexural wave as a transversal wave which contains significant out-of-plane deformation, and the Lucassen wave as a pressure wave in the interface which is dominated by the displacement in the plane of the interface [16].

The factorization Eq. (21) generalizes previous factorizations derived for an interface at a fluid half-space [22, 35, 48]. That a factorization like Eq. (21) does not always hold for physically relevant parameters was already predicted by Lucassen [48], and in the context of a fluid half-space is an established experimental result [8, 49].

III. ANALYTICAL LIMITING CASES

A. Symmetric Scenario

We now assume that media I and III have the same properties, i.e. that $\rho \equiv \rho_{\mathrm{I}} = \rho_{\mathrm{III}}$, $\tilde{g}_s \equiv \tilde{g}_{\mathrm{I},s} = \tilde{g}_{\mathrm{III},s}$, $\tilde{g}_d \equiv \tilde{g}_{\mathrm{I},d} = \tilde{g}_{\mathrm{III},d}$, so that $\alpha \equiv \alpha_{\mathrm{I}} = \alpha_{\mathrm{III}}$, $\lambda_l \equiv \lambda_{\mathrm{I},l} = \lambda_{\mathrm{III},l}$, $\lambda_t \equiv \lambda_{\mathrm{I},t} = \lambda_{\mathrm{III},t}$. In this case, the dispersion relation Eq. (12) simplifies to

$$\begin{aligned} 0 = {} & (k^2\tilde{\Pi}_{2\mathrm{D}} - \omega^2\rho_{2\mathrm{D}})(k^2 - \lambda_l^{-1}\lambda_t^{-1}) \\ & \times \left[(k^2\tilde{g}_{2\mathrm{D}} - i\omega\rho_{2\mathrm{D}})(k^2 - \lambda_l^{-1}\lambda_t^{-1}) + 2i\omega\rho\lambda_l^{-1}\right] \\ & + 2\omega^2\rho\lambda_t^{-1}(k^2\tilde{g}_{2\mathrm{D}} - i\omega\rho_{2\mathrm{D}})(k^2 - \lambda_l^{-1}\lambda_t^{-1}) \\ & - i\omega\tilde{g}_s^2\lambda_l^{-1}\lambda_t^{-1}\left(\alpha^4 - k^2\lambda_l^{-1}\lambda_t^{-1}\right) , \end{aligned} \tag{30}$$

which also factorizes under the assumptions (19), (20), to yield

$$\begin{aligned} 0 = {} & \left[k^2\tilde{\Pi}_{2\mathrm{D}} - \omega^2(\rho_{2\mathrm{D}} + 2\rho\lambda_l)\right] \\ & \times \left[k^2\tilde{g}_{2\mathrm{D}} - i\omega\left(\rho_{2\mathrm{D}} + 2\rho\lambda_t\right)\right]. \end{aligned} \tag{31}$$

This equation follows alternatively from the previous factorization (21), and shows that in the symmetric scenario gravitational acceleration becomes irrelevant. Equating each of the two factors in Eq. (31) with zero yields generalizations of the well-known capillary and Lucassen waves at interfaces separating two identical media [3, 10].

Upon removing the effects related to the surface ($\rho_{2\mathrm{D}} = 0$, $\tilde{g}_{2\mathrm{D}} = 0$, $\tilde{\Pi}_{2\mathrm{D}} = 0$), Eq. (30) becomes

$$k^2\lambda_l^{-1}\lambda_t^{-1} = (k^2 + \lambda_t^{-2})^2 . \tag{32}$$

This relation is very similar to the Rayleigh wave dispersion relation [17–19], which describes surface waves on a viscoelastic half-space, and which we discuss further below. In contrast to the Rayleigh wave dispersion relation for a single half-space, Eq. (32), lacks a factor of 4 on the left-hand side, c.f. Eq. (35) below. In App. C, we plot numerical solutions of Eq. (32) for a Newtonian fluid. We note that by removing the interface from two identical bulk fluid half-spaces, we reduce our setup to an infinite space of one bulk fluid. Nevertheless, the existence of solutions to Eq. (32) indicates that localized waves similar to Rayleigh surface waves can exist along any plane in the bulk of a fluid. As the plots in App. C demonstrate, these waves have a phase velocity $c \sim \omega^{1/2}$ and hence are different from the usual pressure wave in a compressible bulk fluid, for which the phase velocity is independent of the frequency.

B. Asymmetric Scenario

We now consider the asymmetric case, where medium III can be neglected in comparison to medium I. Typically, this is the case when medium I is much denser than medium III. The dispersion relation for this case has been derived before [22], and proceeds similar to Sec. II, but without explicitly taking into account the displacement

above the interface, $z > 0$. The resulting equation is [22]

$$\begin{aligned} 0 = 4 &\left(k^2\tilde{\Pi}_{2\mathrm{D}} + \rho_{\mathrm{I}} g - \omega^2 \rho_{2\mathrm{D}}\right) \\ &\times \left[\left(k^2 \tilde{g}_{2\mathrm{D}} - i\omega\rho_{2\mathrm{D}}\right)\left(k^2 - \lambda_{\mathrm{I},l}^{-1}\lambda_{\mathrm{I},t}^{-1}\right) + i\omega\rho_{\mathrm{I}}\lambda_{\mathrm{I},l}^{-1}\right] \\ &+ 4\left(k^2\tilde{g}_{2\mathrm{D}} - i\omega\rho_{2\mathrm{D}}\right)\omega^2\rho_{\mathrm{I}}\lambda_{\mathrm{I},t}^{-1} \\ &+ \tilde{g}_{\mathrm{I},s}\left[i\omega\tilde{g}_{\mathrm{I},s}\left(-4k^2\lambda_{\mathrm{I},l}^{-1}\lambda_{\mathrm{I},t}^{-1} + (k^2+\lambda_{\mathrm{I},t}^{-2})^2\right)\right. \\ &\left. + 2\rho_{2\mathrm{D}} g k^2\left(2\lambda_{\mathrm{I},l}^{-1}\lambda_{\mathrm{I},t}^{-1} - (k^2+\lambda_{\mathrm{I},t}^{-2})\right)\right] , \end{aligned} \tag{33}$$

This equation also follows from the full dispersion relation Eq. (12) in the limit

$$\frac{\rho_{\mathrm{III}}}{\rho_{\mathrm{I}}} \ll 1, \quad |\lambda_{\mathrm{III},l} k| \approx 1, \quad |\lambda_{\mathrm{III},t}| \lesssim |\lambda_{\mathrm{I},t}| , \tag{34}$$

where $|\lambda_{\mathrm{III},l} k| \approx 1$ is obeyed for a medium III that is almost incompressible.

We now give a short summary of the waves described by Eq. (33), and refer the reader to Ref. [22] for more details.

Upon removing the effects related to the surface ($\rho_{2\mathrm{D}} = 0$, $\tilde{g}_{2\mathrm{D}} = 0$, $\tilde{\Pi}_{2\mathrm{D}} = 0$) and also gravity ($g = 0$), Eq. (33) becomes

$$4k^2\lambda_{\mathrm{I},l}^{-1}\lambda_{\mathrm{I},t}^{-1} = \left(k^2 + \lambda_{\mathrm{I},t}^{-2}\right)^2 , \tag{35}$$

where $\lambda_{\mathrm{I},l}^{-1}$, $\lambda_{\mathrm{I},t}^{-1}$ are given by Eqs. (8), (9). This is the classical Rayleigh conditional equation [17] whose solutions lead to the known (viscoelastic) Rayleigh waves [18, 19].

Similarly to Sec. II C, the conditional equation (33) factorizes if the approximations Eqs. (19), (20), hold for the half-space. Equation (33) then becomes

$$\begin{aligned} 0 = &\left[k^2\tilde{\Pi}_{2\mathrm{D}} + \rho_{\mathrm{I}} g - \omega^2(\rho_{2\mathrm{D}} + \rho_{\mathrm{I}}\lambda_{\mathrm{I},l})\right] \\ &\times \left[k^2\tilde{g}_{2\mathrm{D}} - i\omega\left(\rho_{2\mathrm{D}} + \rho_{\mathrm{I}}\lambda_{\mathrm{I},t}\right)\right] , \end{aligned} \tag{36}$$

which equivalently follows from Eq. (21) in the limit Eq. (34). By equating each of the factors of Eq. (36) with zero, we obtain two equations which correspond to two different wave solutions [22]. The first factor yields a generalization of the capillary-gravity-flexural surface wave, the second a generalization of the Lucassen wave. As has been shown before, for high frequencies the factorization Eq. (36) can break down, and a frequency-dependent transition from the Lucassen wave to a Rayleigh wave can occur [22].

For an incompressible Newtonian fluid, the second factor in Eq. (36), which corresponds to the Lucassen wave solution, has been shown to be the Fourier transform of a fractional wave equation [16]. Using a simplified system that describes interfacial pressure waves in elastic monolayers at the water-air interface via coupling a one-dimensional wave equation, representing the dynamics of the interface, to a parabolic equation on the half-space below, a mathematically rigorous limit leading to a fractional wave equation is presented in Ref. [50].

C. Free Membrane

To obtain the dispersion relation for a free membrane in vacuum, we consider a limit of Eq. (33) in which medium I is negligible compared to the interface. This is the case if

$$\frac{\rho_{\mathrm{I}}\lambda_{\mathrm{I},t}}{\rho_{2\mathrm{D}}} \ll 1, \qquad \frac{\rho_{\mathrm{I}}\lambda_{\mathrm{I},l}}{\rho_{2\mathrm{D}}} \ll 1, \tag{37}$$

which means that the oscillating mass of the motion below the membrane is negligible compared to the membrane excess mass density. The conditional equation (33) then factorizes as

$$0 = (k^2\tilde{\Pi}_{2\mathrm{D}} - \omega^2\rho_{2\mathrm{D}})(k^2\tilde{g}_{2\mathrm{D}} - i\omega\rho_{2\mathrm{D}}) , \tag{38}$$

which is alternatively obtained from Eq. (36) in the limit Eq. (37).

Equating the first factor in Eq. (38), which comes from the capillary wave factor in Eq. (36), with zero and substituting the definition of $\tilde{\Pi}_{2\mathrm{D}}$, Eq. (14), yields

$$-\kappa_{2\mathrm{D}}(-ik)^4 + \eta_{2\mathrm{D}}^{\perp}(-i\omega)(-ik)^2 + \sigma_{2\mathrm{D}}(-ik)^2 = \rho_{2\mathrm{D}}(-i\omega)^2 , \tag{39}$$

which is a generalization of the classical dispersion relation of a bending wave in an elastic plate [43], recovered in the limit $\eta_{2\mathrm{D}}^{\perp} = 0$, $\sigma_{2\mathrm{D}} = 0$. If the first factor of Eq. (38) is equal to zero, it can be seen directly from the system of equations used to derive the general dispersion relation in App. B that $\Phi = 0$ in Eq. (6), so that the displacement field $\boldsymbol{u}$ corresponding to the dispersion relation Eq. (39) is purely transversal.

Using the definition of $\tilde{g}_{2\mathrm{D}}$, Eq. (13), and equating the second factor of Eq. (38) with zero, yields a one-dimensional wave equation

$$(-ik)^2 K_{2\mathrm{D}} + (-i\omega)(-ik)^2\eta_{2\mathrm{D}} = (-i\omega)^2\rho_{2\mathrm{D}} . \tag{40}$$

If Eq. (40) holds, it can be seen from the system of equations used to derive the general dispersion relation in App. B that $\Psi = 0$ in Eq. (7), so that the displacement field $\boldsymbol{u}$ is purely longitudinal. Thus, while in general both the longitudinal and transversal displacements in Eq. (3) are necessary to fulfill momentum conservation and the boundary conditions, for a membrane in vacuum the two fields decouple.

IV. EXAMPLE SYSTEMS

A. Newtonian fluid as bulk medium

1. *Viscoelastic relaxation functions for compressible Newtonian fluid*

To apply our theory to situations where water is at least one of the bulk media and gravity is present, we need to relate the viscoelastic stress-strain relation (2) to

the usual stress-strain relation for a compressible Newtonian fluid. This is done by including gravity, modeled as an external force $F_i = -\delta_{iz}\rho g$, into the argumentation usually carried out to derive sound waves in bulk media [3, 4, 46], see Ref. [22] for more details. For a compressible Newtonian fluid, the relaxation functions follow as

$$\tilde{g}_{M,s}(\omega) = 2\eta_M, \tag{41}$$

$$\tilde{g}_{M,d}(\omega) = 3\eta'_M + \frac{3K_M}{-i\omega}, \tag{42}$$

where η_M, η'_M are the shear- and dilational viscosity of medium M, and K_M is the modulus of compression (bulk modulus) of the fluid, which for adiabatic compression is related to the sound velocity c_M as $K_M = \rho_M c_M^2$ [3]. The relaxation function Eq. (42) describes the response of a Kelvin-Voigt material and switches from a predominantly elastic to a viscous response if ω exceeds the crossover frequency

$$\omega_{M,d} \equiv \frac{K_M}{\eta'_M} \ . \tag{43}$$

For the effect of gravity, we use the surface gravity approximation [46], for which effects of gravity only enter in the boundary conditions at $z = 0$, c.f. App. B.

If the Newtonian fluid is weakly compressible, such that η_M, $\eta'_M \ll 3K_M/\omega$, then the factorization conditions Eq. (19) become

$$\frac{K_M}{3\omega} \gg \frac{\omega\rho_M}{|k|^2} \gg \frac{\eta_M}{2}. \tag{44}$$

Substituting the relaxation functions Eqs. (41), (42), into the generalized capillary-gravity dispersion relation Eq. (23), we obtain

$$\tilde{\Pi}_{2D}k^2 = \omega^2\left(\frac{\rho_I + \rho_{III}}{k} + \rho_{2D}\right) - (\rho_I - \rho_{III})g \ , \tag{45}$$

where we use that $\lambda_{M,l}^{-1} \approx k$ holds in the limit Eq. (44). If $\tilde{\Pi}_{2D} \approx \sigma_{2D}$, then Eq. (45) is the classical dispersion relation for capillary-gravity waves for Newtonian fluids [51].

On the other hand, the Lucassen dispersion relation Eq. (26) yields

$$k^2 = \frac{i\omega}{\tilde{g}_{2D}}\left(\sqrt{\frac{\rho_I\eta_I}{-i\omega}} + \sqrt{\frac{\rho_{III}\eta_{III}}{-i\omega}} + \rho_{2D}\right) \ . \tag{46}$$

Substituting the definition of $\tilde{g}_{2D}$ (13) into Eq. (46), we obtain

$$k = \sqrt{\frac{\rho_{2D}\omega^2 + e^{i\pi/4}\left(\sqrt{\rho_I\eta_I\omega^3} + \sqrt{\rho_{III}\eta_{III}\omega^3}\right)}{K_{2D} - i\omega\eta_{2D}}} \ , \tag{47}$$

where we have chosen the complex square root that leads to a positive real part for k, so that the resulting wave propagates in the positive x-direction. This is a generalization of the Lucassen dispersion relation [9–12], which was originally derived for a half-space filled with an incompressible Newtonian fluid, and without taking into account interfacial inertia. Upon neglecting the membrane viscosity, $\eta_{2D} = 0$, Eq. (47) reduces to one central result from Ref. [38], where the Lucassen wave was discussed for elastic interfaces separating two Newtonian fluids.

For future reference, we note that for the Lucassen wave on a Newtonian fluid, the crossover frequency at which the interfacial inertia dominates over the bulk fluid inertia is obtained by substituting the shear relaxation function Eq. (41) into Eq. (28), which yields

$$\omega_{2D}^{\rho} = \left(\frac{\sqrt{\rho_I\eta_I} + \sqrt{\rho_{III}\eta_{III}}}{\rho_{2D}}\right)^2 \ . \tag{48}$$

For angular frequencies above ω_{2D}^{ρ}, the Lucassen wave behaves thus like the one-dimensional wave equation solution for a free membrane, Eq. (40). This will be used to estimate crossover frequencies in Sec. IV.

2. *Water-Water Interface*

The Newtonian fluid model deserves further attention, since water, which is ubiquitous and fundamentally important for life on earth, is very well described as a Newtonian fluid up to angular frequencies slightly below the THz regime [52–55], as we discuss further below.

We consider water at 25 °C for medium I und III, and use the parameters [56] $\eta \approx 1\cdot10^{-3}$ Pa · s, $\eta' \approx 3\cdot10^{-3}$ Pa · s, $\rho \approx 1\cdot10^{3}$ kg/m^3, $c_I \approx 1.5\cdot10^{3}$ m/s. For the interface, we use the parameters $g = 9.81$ m/s^2, $\rho_{2D} = 1\cdot10^{-6}$ kg/m^2, $\eta_{2D} = 1\cdot10^{-9}$ Pa · s · m, $\eta'_{2D} = 0$, $\eta^{\perp}_{2D} = 1\cdot10^{-9}$ Pa · s · m, $K_{2D} = 34\cdot10^{-3}$ N/m, $\sigma_{2D} = 5\cdot10^{-3}$ N/m, $\kappa_{2D} = 3\cdot10^{-19}$ N·m, appropriate for a planar DPPC bilayer immersed in water. The values for σ_{2D} and K_{2D} are obtained for monolayers via measuring Langmuir isotherms [14, 57], the shear viscosity η_{2D} for a DPPC bilayer is estimated from measurements of diffusing lipids in lipid membranes [58, 59], while the bending rigidity κ_{2D} is extracted from weakly deforming bilayer vesicles [60, 61]. Although the values for σ_{2D} and K_{2D} are obtained for monolayers, we assume for our numerical study that the corresponding values for a bilayer are comparable. For the transverse membrane viscosity $\eta^{\perp}_{2D}$, we did not find any experimentally measured values for a DPPC membrane in the literature; we therefore use the same value as for η_{2D}. For Langmuir monolayers in a trough, the area mass density ρ_{2D} can be calculated as the quotient of added lipid mass and trough area. We use a typical value for DPPC monolayers in the context of surface wave measurements [14].

The Newtonian fluid model Eqs. (41), (42) describes bulk water in a limited frequency range, and starts to break down on time scales comparable to those of the individual fluid molecules [52–55]. For example, the shear

response starts to deviate from Eq. (41) at frequencies $\omega \gtrsim 10^{11}$ /s [52–55], and similar effects are expected for the dilational response; in fact, as we will see below, the dilational crossover frequency Eq. (43) is of the order of 10^{11} /s for water. Likewise, for molecular length scales we expect that the assumption of a homogeneous medium will break down [52], and that the dependence of the fluid response on the distance from the interface will become relevant [62]. Therefore, while our analysis below extends to angular frequencies $\omega = 10^{14}$ /s, the high-frequency range $\omega = 10^{11}$ to $\omega = 10^{14}$ /s is included primarily to study the mathematical behavior of the dispersion relation, and is not expected to accurately describe the response of actual water in an experimental system.

To validate the factorization Eq. (31), we numerically solve the full dispersion relation Eq. (12) for k for a wide range of frequencies ω. For the two distinct solutions for $k(\omega)$ that we find, we calculate the phase velocities and propagation distances via Eqs. (15), (16). In Fig. 2 (a) we compare the results to phase velocities and propagation distances obtained from numerical solutions of the factorized dispersion relation, Eq. (31), which for a Newtonian fluid are given by Eqs. (45), (47) with $\rho \equiv \rho_{\mathrm{I}} = \rho_{\mathrm{III}}$, $\eta \equiv \eta_{\mathrm{I}} = \eta_{\mathrm{III}}$.

The phase velocity of one numerical solution of the full dispersion relation Eq. (12) agrees with the capillary-gravity-flexural wave dispersion relation Eq. (45) for most of the frequency range considered. For angular frequencies $\omega \ll 10^7$ /s, the bulk inertia dominates over the interfacial inertia in Eq. (45), so that $k^3 \approx 2\omega^2\rho/\sigma_{2\mathrm{D}}$, where we use that for the frequencies and wave numbers in that regime it holds that $\tilde{\Pi}_{2\mathrm{D}} \approx \sigma_{2\mathrm{D}}$. This approximate expression for k implies $k \sim \omega^{2/3}$, and consequently $c = \omega/k \sim \omega^{1/3}$, as observed in the figure. According to Eq. (24), at the crossover frequency $\omega^{\sigma}_{2\mathrm{D}} \equiv \sigma_{2\mathrm{D}}/\eta^{\perp}_{2\mathrm{D}} = 5 \cdot 10^6$ /s, the viscous dissipation term in the interfacial response $\tilde{\Pi}_{2\mathrm{D}}$ starts to dominate over the surface tension, so that $\tilde{\Pi}_{2\mathrm{D}} \approx -i\omega\eta^{\perp}_{2\mathrm{D}}$. The right-hand side of Eq. (45) is still dominated by the bulk inertia, so that $k \sim \omega^{1/3}$, and hence $c \sim \omega^{2/3}$, as indicated in Fig. 2 (a) by a black bar. Finally, at $\omega_d \equiv K/\eta' = 5 \cdot 10^{11}$ /s, the dilational viscosity starts to dominate over the elastic response in Eq. (42); the compressibility of the fluid starts to become more relevant, and the solution corresponding to the capillary-flexural wave seizes to exist at $\omega^{\mathrm{max}}_{\mathrm{CG}} \approx 3.4 \cdot 10^{11}$/s. While this breakdown of the capillary-flexural wave is an interesting mathematical fact, we emphasize again that at frequencies in the THz regime, the assumption that water behaves as a Newtonian fluid breaks down, and Eqs. (41), (42), need to be amended to get a physically accurate description of the viscoelastic properties of water at such high frequencies [52–55]. The phase velocity of the second solution of Eq. (12) agrees with the Lucassen wave dispersion relation Eq. (47) almost perfectly throughout the frequency range considered, except for a discontinuity at the frequency $\omega_d = 5 \cdot 10^{11}$ /s, where the dilational bulk response switches from elasticity dominated to viscous. The crossover frequencies Eqs. (29), (48), associated with the Lucassen wave are given by $\omega^{\rho}_{2\mathrm{D}} = 4 \cdot 10^{12}$ /s, $\omega^{\mathrm{elastic}}_{2\mathrm{D}} = 3.4 \cdot 10^7$ /s. For frequencies $\omega \ll \omega^{\mathrm{elastic}}_{2\mathrm{D}}$, the Lucassen wave dispersion relation is thus approximately given by $K_{2\mathrm{D}}k^2 \approx 2e^{i\pi/4}\sqrt{\rho\eta\omega^3}$, so that $k \sim \omega^{3/4}$ and hence $c \sim \omega^{1/4}$, as shown by a black bar in Fig. 2 (a). At the crossover frequency $\omega^{\mathrm{elastic}}_{2\mathrm{D}}$, the interfacial viscosity starts to dominate over the interfacial elasticity, so that $-i\omega\eta_{2\mathrm{D}}k^2 \approx 2e^{i\pi/4}\sqrt{\rho\eta\omega^3}$, and hence $k \sim \omega^{1/4}$, which implies $c \sim \omega^{3/4}$, as observed approximately in Fig. 2 (a). The slight deviations from the expected scaling might indicate that the factorization condition does not hold perfectly in this regime. For very large frequencies $\omega \gg \omega^{\rho}_{2\mathrm{D}}$, the Lucassen dispersion relation approximately yields $k^2 \approx i\omega\rho_{2\mathrm{D}}/\eta_{2\mathrm{D}}$, meaning $k \sim \omega^{1/2}$ from which we obtain $c \sim \omega^{1/2}$. The onset of this regime can be observed at the highest frequencies shown in Fig. 2 (a).

In Fig. 2 (c) we show the propagation distances β^{-1}, defined in Eq. (16), corresponding to the solutions of both the full and factorized dispersion relations; we calculate the propagation distances using the same complex wave numbers $k(\omega)$ as used for Fig. 2 (a). Overall, both the factorized capillary-flexural wave and the Lucassen wave propagation distances agree with the full solution, and show scalings fully consistent with Eqs. (17), (18) and the local scalings of k with ω discussed in the context of Fig. 2 (a). The only exception to this is the low-frequency regime of the capillary-flexural wave, where the factorized dispersion relation Eq. (45) predicts a propagation distance orders of magnitude larger as compared to the full dispersion relation Eq. (12). Furthermore, the expected scaling of $\beta^{-1} \sim \omega^{-2/3}$ for the capillary-gravity-flexural wave for angular frequencies $\omega \ll 10^7$/s does not fit perfectly to the prediction of Eq. (12), so that real and imaginary parts of $k(\omega)$ scale differently with ω in this regime. This shows that while the factorized dispersion relation Eq. (45) captures the real part of the wave number properly, for the imaginary part the full dispersion relation is necessary.

3. *Air-Water Interface*

Experiments on lipid monolayers often measure membrane properties on a trough of water [8, 13–15], which corresponds to a planar viscoelastic interface with water and air as bulk materials I and III. In theoretical modeling of air-water interfaces, one usually only considers the water dynamics below the membrane, and does not explicitly consider the dynamics of the air above. In this section, we compare predictions of our full dispersion relation Eq. (12) to the factorized half-space dispersion relation Eq. (36), to demonstrate that the air dynamics can indeed be neglected.

For medium I we use water, modeled as a compressible Newtonian fluid with the parameters from Sec. IV A 2.

To model air as medium III, we also use the compressible Newtonian fluid model from Sec. IV A 1; at 25 °C, the relevant parameters are [56] $\eta_{\mathrm{III}} \approx 18.2 \cdot 10^{-6}$ Pa·s, $\eta'_{\mathrm{III}} = 0$, $\rho_{\mathrm{III}} \approx 1.2$ kg/m^3, $c_{\mathrm{III}} \approx 343$ m/s.

For a wide range of frequencies, we numerically solve both the full dispersion relation Eq. (12) and the dispersion relations pertaining to each of the two factors of the half-space dispersion relation Eq. (36). We subsequently use Eqs. (15), (16), to evaluate the corresponding phase velocities and propagation distances, and show the results in Fig. 2 (b), (d). For comparison, we also include the capillary-gravity-flexural wave solution of the full dispersion relation in the asymmetric case Eq. (33).

For the capillary-gravity-flexural wave, we observe that the phase velocities predicted by the full dispersion relation agree perfectly with the asymmetric dispersion relation throughout, and with the factorized half-space dispersion relation up until $\omega_{\mathrm{I},d} \equiv K_{\mathrm{I}}/\eta'_{\mathrm{I}} = 5 \cdot 10^{11}$ /s; at this frequency, the dilational response of the water below the interface becomes dominated by the viscosity, and at $\omega_{\mathrm{CG}}^{\max} = 3.41 \cdot 10^{11}$ /s the capillary-gravity-flexural wave solution disappears, similar to the symmetric case discussed in Sec. IV A 2 above. In contrast to the symmetric case, for the half-space, the phase velocity is not monotonic, but has a minimum at $\omega \approx 10^2$ /s. This minimum denotes the crossover from capillarity-dominated to gravity-dominated dispersion, and its location follows from Eq. (45), by equating the left-hand side of the equation with the gravitational term, as

$$\omega_{\mathrm{CG}} = \left(\frac{(\rho_{\mathrm{I}} - \rho_{\mathrm{III}})^3 \cdot g^3}{(\rho_{\mathrm{I}} + \rho_{\mathrm{III}})^2 \cdot \sigma_{\mathrm{2D}}} \right)^{1/4} \approx 117 \text{ /s} , \tag{49}$$

where we use that for the frequencies and wave numbers involved $\tilde{\Pi}_{\mathrm{2D}} \approx \sigma_{\mathrm{2D}}$ holds, as follows from Eq. (14), and employ the gravity-wave dispersion relation (see just below) to eliminate k from the equation. For frequencies $\omega \ll \omega_{\mathrm{CG}}$, the right-hand side of the dispersion relation Eq. (45) is dominated by the gravitational term, so that $k \approx \omega^2/g \cdot (\rho_{\mathrm{I}} + \rho_{\mathrm{III}})/(\rho_{\mathrm{I}} - \rho_{\mathrm{III}}) \sim \omega^2$. According to Eq. (18), we thus have $c \sim \omega^{-1}$, as observed in Fig. 2 (b). This gravity-wave regime is not present in the symmetric scenario, because for $\rho_{\mathrm{I}} = \rho_{\mathrm{III}}$ the rightmost term in Eq. (45) vanishes. For the phase velocity of the Lucassen wave solution, we observe very good agreement between the full dispersion relation and the factorized half-space solution throughout. Even close to the frequency $\omega_{\mathrm{CG}}^{\max} = 3.41 \cdot 10^{11}$/s, where the capillary-gravity-flexural wave solution disappears, the factorized Lucassen dispersion relation does not deviate from the full dispersion relation. This is in contrast to the symmetric scenario shown in Fig. 2 (a), and presumably because, in the present case, $\omega_{\mathrm{CG}}^{\max} = 3.41 \cdot 10^{11}$ /s is closer to the crossover frequency $\omega_{\mathrm{2D}}^{\rho} = 10^{12}$ /s, at which the inertia of the interface starts to dominate over bulk properties, so that the crossover in the bulk viscoelastic response is already less relevant for the dispersion relation.

The propagation distance of the capillary-gravity-flexural wave, shown in Fig. 2 (d), displays a behavior similar to the symmetric case depicted in Fig. 2 (c): For frequencies above $\omega_{\mathrm{2D}}^{\sigma} \equiv \sigma_{\mathrm{2D}}/\eta_{\mathrm{2D}}^{\perp} = 5 \cdot 10^6$ /s, where the surface viscosity dominates over the surface tension, the propagation distance of the full capillary-gravity-flexural wave agrees with the factorized half-space results. Below the crossover frequency $\omega_{\mathrm{2D}}^{\sigma}$, the two formulas Eqs. (12), (36) predict different propagation distances. The propagation distance predicted by the full dispersion relation of the asymmetric case Eq. (33) agrees with the full dispersion relation even below $\omega_{\mathrm{2D}}^{\sigma}$, except for very low frequencies $\omega \lesssim 10^2$ /s. Also note that the propagation distances β^{-1} of the capillary-gravity-flexural wave scale differently than $\beta^{-1} \sim \omega^{-2}$, as observed in Fig. 2 (d).

To summarize this section, for an air-water interface, the factorized half-space dispersion relation Eq. (36) overall constitutes a good approximation to the full dispersion relation Eq. (12) for both capillary-gravity-flexural and Lucassen wave. However, for the capillary-gravity-flexural wave, the factorized equation fails to predict the breakdown of the wave at high frequencies, and overestimates the propagation distances at low frequencies.

B. Viscoelastic Bulk Media

One advantage of both our general dispersion relation Eq. (12), and the factorization Eq. (21), is that these relations are derived for arbitrary linear, homogeneous, isotropic viscoelastic bulk media. While in the previous Sec. IV A we used Newtonian fluids as bulk media, in the present section we consider interfacial waves for two other viscoelastic bulk materials.

More explicitly, we consider the dispersion relation of the Lucassen wave solution on polymer gels and polymer solutions as bulk media. We here focus on the Lucassen wave, as this is the relevant pressure wave for biological scenarios related to nerve pulse propagation [15, 16]. In particular, a viscoelastic membrane surrounded by two viscoelastic media serves as a model for the cell membrane of a neuron, separating the hydrogel axoplasm and extracellular fluid.

1. *Polymer gels as bulk media: Kelvin-Voigt model*

The elastic properties of polymer gels are determined by the density of entanglements between individual polymer chains. A characteristic of a gel are the extremely long lifetimes of entanglements. On timescales relevant to the wave phenomena we investigate, we can therefore assume permanent crosslinks between chains [63]. In the linear regime, the polymer gel can thus be modeled as a purely elastic polymer network immersed in a viscous Newtonian solvent. We model this as a Kelvin-Voigt material. For this, we leave the dilational relaxation func-

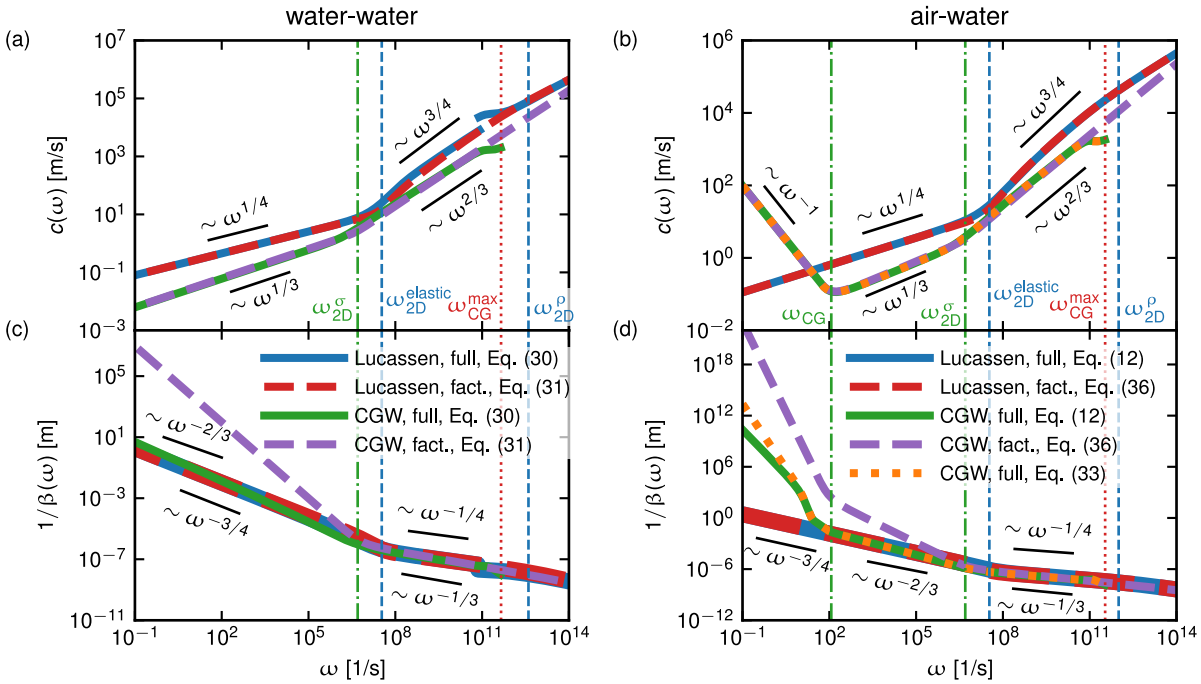

FIG. 2. (a), (c) Properties of waves at an interface separating two Newtonian fluids with identical parameters, as discussed in Sec. IV A 2. Parameters are given in Sec. IV A, and correspond to a DPPC membrane (interface) and water (bulk). The full dispersion relation Eq. (30) and the equations that correspond to the individual factors of the factorized symmetric dispersion relation Eq. (31) are solved numerically, to obtain the wave number k as a function of ω. The corresponding (a) phase velocity and (c) propagation distance is then calculated using Eqs. (15), (16). (b), (d) Phase velocities and propagation distances for an air-water interface, as discussed in Sec. IV A 3. Both the full dispersion relation Eq. (12) and the equations corresponding to the individual factors of the factorized asymmetric dispersion relation Eq. (36) are solved numerically, and the resulting wavenumber $k(\omega)$ is used to calculate c, β^{-1} via Eqs. (15), (16). Additionally, the solution of the asymmetric vacuum-water dispersion relation (33) is shown for comparison. For all subplots, vertical dashed lines denote the various crossover frequencies discussed for (a), (c) in Sec. IV A 2, and for (b), (d) in Sec. IV A 3; while green dash-dotted lines denote crossovers in the capillary-gravity wave, blue dashed lines indicate crossovers in the Lucassen wave. Red dotted lines highlight the frequencies at which solutions of the full dispersion relation disappear. The power-law scalings of c and β^{-1} within each scaling regime are indicated by black bars.

tion (42) unchanged, and use a shear relaxation function

$$\tilde{g}_{M,s}(\omega) = 2\eta_M + \frac{2E_M}{-i\omega} \,, \tag{50}$$

where η_M is the fluid viscosity, while E_M is the fluid elastic modulus under shear. A systematic bottom-up theory for the linear frequency-dependent viscoelastic response of a polymeric network can be found in Ref. [64].

The Kelvin-Voigt material has a characteristic crossover frequency

$$\omega_M^{\mathrm{KV}} = \frac{E_M}{\eta_M} \,, \tag{51}$$

below which the shear response is dominated by elasticity, $\tilde{g}_{M,s}(\omega) \approx 2E_M/(-i\omega)$. Above the crossover frequency ω_M^{KV}, the shear response is approximately that of a Newtonian fluid, $\tilde{g}_{M,s}(\omega) \approx 2\eta_M$.

Starting from the analytical solution of the generalized Lucassen-wave Eq. (26) and inserting the shear relaxation function Eq. (50) for $\lambda_{M,t}$ in Eq. (9), we obtain the analytical Lucassen-wave solution for a viscoelastic membrane at the interface of two polymer gels as

$$k = \sqrt{\frac{\rho_{2\mathrm{D}}\omega^2 + e^{i\pi/4}\left(\sqrt{R_{\mathrm{I}}(\omega)} + \sqrt{R_{\mathrm{III}}(\omega)}\right)}{K_{2\mathrm{D}} - i\omega\eta_{2\mathrm{D}}}} \,, \tag{52}$$

where

$$R_M(\omega) = \rho_M\eta_M\omega^3\left(1 + i\frac{\omega_M^{\mathrm{KV}}}{\omega}\right) \,, \tag{53}$$

and where all complex square roots are chosen to have positive real part. For $\omega \gg \omega_M^{\mathrm{KV}}$, we have $R_M(\omega) \approx \rho_M\eta_M\omega^3$ and Eq. (52) reduces to the Lucassen dispersion relation for a Newtonian fluid, Eq. (47).

As an explicit example we consider a symmetric system with Kelvin-Voigt bulk media, with elastic moduli $E \equiv E_{\mathrm{I}} = E_{\mathrm{III}} = 0.1$ Pa, as in Ref. [63]. For the other bulk and interface parameters we use the same as in Sec. IV A 2; according to Eq. (51), this results in a Kelvin-Voigt crossover frequency $\omega^{\mathrm{KV}} = 10^2$ /s.

In Fig. 3 (a), (c), we compare the predictions of Eq. (52) to both the full symmetric dispersion relation Eq. (30), and the factorized Lucassen relation Eq. (47) for a symmetric Newtonian fluid system. As expected, for $\omega \gg \omega_M^{\mathrm{KV}}$ the two factorized solutions Eqs. (47), (52), lead to indistinguishable phase velocities and propagation distances, and differ only for $\omega \lesssim \omega_M^{\mathrm{KV}}$, when the elastic component in Eq. (50) is non-negligible. A solution that is similar to the Lucassen wave for the full dispersion relation Eq. (30) exists only in the frequency range $\omega > \omega_{\mathrm{KV}}^{\mathrm{min}} = 2.29$ /s, where it is well-described by Eq. (52), except for a discontinuity at the frequency $\omega = 8.4{\cdot}10^{10}$ /s, as observed in Sec. IV A 3. To rationalize the low-frequency breakdown of the Lucassen wave, we show in App. D, that as ω approaches $\omega_{\mathrm{KV}}^{\mathrm{min}} = 2.29/\mathrm{s}$ from above, the real part of λ_t^{-1} approaches zero, so that the transversal decay length of the Lucassen wave diverges. The wave solution therefore does not decay any longer away from the interface, and hence ceases to be a surface wave solution.

In summary, we observe that the Lucassen wave breaks down for angular frequencies shortly below $\omega_{\mathrm{KV}}^{\mathrm{min}}$, when the bulk media responds predominantly elastically. For angular frequencies above $\omega_{\mathrm{KV}}^{\mathrm{min}}$, the Lucassen wave behaves as the corresponding wave solution for purely viscous fluids, as seen in Fig. 2 (a), (c), and in particular displays the same scaling regimes.

2. *Polymer solutions as bulk media: Maxwell model*

In contrast to the polymeric gel, the elastic properties of a solution of rather short polymer chains in liquid solvent are determined by finite lifetime interchain entanglements. Polymer chains may disentangle themselves from neighboring chains by diffusion, a process called reptation [63]. The characteristic time of a chain to diffuse out of the loose polymer network is called reptation time, and the characteristic macroscopic stress relaxation time $\tau_M \equiv 1/\omega_M^{\mathrm{MW}}$ of such a polymer solution scales directly with the reptation time [63]. Polymer solutions can be modeled as a Maxwell fluid with shear relaxation function

$$\tilde{g}_{M,s}(\omega) = \frac{2\eta_M}{1 - i\omega\tau_M} \ , \tag{54}$$

which for small angular frequency $\omega \ll \omega_M^{\mathrm{MW}} = 1/\tau_M$ reduces to the Newtonian fluid model Eq. (41). It should be noted that real polymer gels are in fact described by more than two viscoelastic regimes and must be modeled by a combination of Kelvin-Voigt and Maxwell models.

The relevance of the Maxwell model goes beyond polymer solutions: As mentioned in Sec. IV A 2, in the THz regime also pure water deviates from a Newtonian fluid model, and descriptions of water on such short timescales are based on the Maxwell model and generalizations thereof [55]. For high-concentration glycerol solutions, non-Newtonian behavior in the shear viscosity can be observed at lower frequencies, namely in the GHz regime [55].

Substituting the Maxwell-model shear relaxation function into the generalized Lucassen-wave Eq. (26), we obtain

$$k = \sqrt{\frac{\rho_{2\mathrm{D}}\omega^2 + e^{i\pi/4}\left(\sqrt{\frac{\rho_{\mathrm{I}}\eta_{\mathrm{I}}\omega^3}{1-i\omega\tau_{\mathrm{I}}}} + \sqrt{\frac{\rho_{\mathrm{III}}\eta_{\mathrm{III}}\omega^3}{1-i\omega\tau_{\mathrm{III}}}}\right)}{K_{2\mathrm{D}} - i\omega\eta_{2\mathrm{D}}}} \ , \tag{55}$$

which for $\omega \ll \omega_M^{\mathrm{MW}} \equiv 1/\tau_M$ reduces to the dispersion relation Eq. (47) of a Newtonian fluid.

As an example, we consider a symmetric system with Maxwell fluids as bulk media. For the characteristic Maxwell frequency we use $\omega^{\mathrm{MW}} \equiv \omega_{\mathrm{I}}^{\mathrm{MW}} = \omega_{\mathrm{III}}^{\mathrm{MW}} = 10^3/\mathrm{s}$, so that $\tau \equiv 1/\omega^{\mathrm{MW}} \equiv \tau_{\mathrm{I}} = \tau_{\mathrm{III}} = 10^{-3}\,\mathrm{s}$. For all other bulk and interface parameters we consider the same values as in Sec. IV A 2.

In Fig. 3 (b), (d), we compare phase velocities and propagation distances based on Eq. (55) to those obtained from the full symmetric dispersion relation Eq. (30) and the Lucassen wave dispersion relation for a Newtonian fluid, Eq. (47). For frequencies $\omega \ll \omega^{\mathrm{MW}}$, where the Maxwell fluid behaves like a Newtonian fluid, all three dispersion relations lead to identical phase velocities and propagation distances, with a scaling that follows from Eqs. (17), (18), and the classical Lucassen wave scaling $k \sim \omega^{3/4}$, as previously observed in Fig. 2 (a), (c). For frequencies $\omega \gg \omega^{\mathrm{MW}}$, the approximate scaling behavior of Eq. (55) can be obtained by considering the numerator and denominator inside the square root separately. We first consider the numerator. Using Eq. (28), and approximating $\tilde{g}_s \approx 2\eta/(-i\omega\tau)$ as appropriate for $\omega \gg \omega^{\mathrm{MW}}$, the crossover from bulk-dominated to interface-dominated inertia occurs at the angular frequency $\omega_{2\mathrm{D}}^{\rho} = 2\sqrt{\rho\eta/\tau}/\rho_{2\mathrm{D}} \approx 6.3 \cdot 10^7/\mathrm{s}$; this crossover here occurs at a significantly lower frequency as compared to a Newtonian fluid with the same density and viscosity, for which in Sec. IV A 2 we obtained 10^{12}/s. The crossover from elastic to viscous interface response, described by the denominator of the dispersion relation Eq. (55), follows via Eq. (29) as $\omega_{2\mathrm{D}}^{\mathrm{elastic}} = K_{2\mathrm{D}}/\eta_{2\mathrm{D}} = 3.4 \cdot 10^7/\mathrm{s}$, which for our system parameters is very close to $\omega_{2\mathrm{D}}^{\rho}$. For $\omega^{\mathrm{MW}} \ll \omega \ll \omega_{2\mathrm{D}}^{\mathrm{elastic}}, \omega_{2\mathrm{D}}^{\rho}$, the dispersion relation is dominated by bulk inertia and interface elasticity; the wave number scales approximately as $k \sim (\sqrt{\rho\eta/\tau}\omega/K_{2\mathrm{D}})^{1/2} \sim \omega^{1/2}$, which according to Eq. (18) implies $c \sim \omega^{1/2}$, $\beta^{-1} \sim \omega^{-1/2}$. In this non-Newtonian frequency regime, the dispersion relations Eqs. (55), (30) agree perfectly, and are markedly different from the Newtonian fluid Eq. (47). For $\omega \gg \omega_{2\mathrm{D}}^{\mathrm{elastic}}, \omega_{2\mathrm{D}}^{\rho}$, the Lucassen wave is dominated by interfacial inertia and interface viscosity, and the wave number scales as $k \sim \sqrt{\rho_{2\mathrm{D}}\omega/\eta_{2\mathrm{D}}} \sim \omega^{1/2}$, so that the scaling $c \sim \omega^{1/2}$, $\beta^{-1} \sim \omega^{-1/2}$ also holds at this frequency. That the dispersion relation is dominated by the interface for high frequencies is highlighted by the free-interface dispersion relation Eq. (40), which is also shown in Fig. 3 (b), (d), and which agrees with the Maxwell dispersion relations

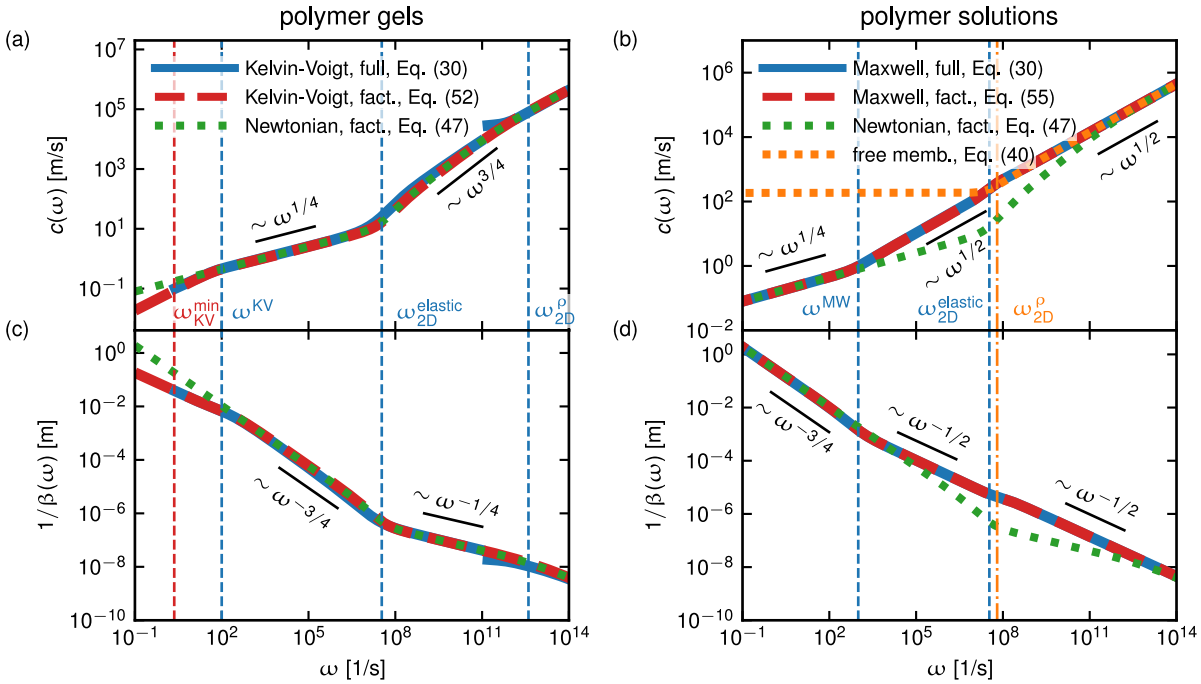

FIG. 3. Phase velocities c and propagation distances β^{-1} for Lucassen waves at an interface separating viscoelastic materials. Phase velocities and propagation distances are obtained from $k(\omega)$ via Eqs. (15), (16). For (a), (c), the viscoelastic bulk materials are two Kelvin-Voigt materials with identical properties, as discussed in Sec. IV B 1. To obtain $k(\omega)$, the full symmetric dispersion relation Eq. (30), the Kelvin-Voigt Lucassen dispersion relation Eq. (47), and the Newtonian-fluid Lucassen relation Eq. (47), are evaluated numerically. For (b), (d), two Maxwell fluids with identical parameters are considered as bulk materials, c.f. Sec. (IV B 2). To obtain $k(\omega)$, each of the dispersion relations Eqs. (30), (40), (47), (52), (55), is evaluated numerically. For all subplots, vertical dashed lines denote crossover frequencies as discussed in Sec. IV B 1 for (a), (c), and in Sec. IV B 2 for (b), (d). Blue dashed lines denote crossovers in the Lucassen wave. Red dashed lines highlight the frequencies at which solutions of the full dispersion relation disappear. The crossover to the free membrane limit is colored orange for better distinguishability. The power-law scalings of c and β^{-1} within each scaling regime are indicated by black bars.

for $\omega \gg \omega_{2D}^{\text{elastic}}, \omega_{2D}^{\rho}$. The interface dominance is also the reason why the Newtonian-fluid dispersion relation starts to agree with the Maxwell-fluid dispersion relation again at the highest frequencies shown: The bulk properties are simply not relevant anymore.

In Fig. 4, we show a phase diagram illustrating the crossover frequencies of the Lucassen wave solution for a viscoelastic membrane surrounded by two half-spaces consisting of a polymer solution in water, described by a Maxwell-fluid model, where we denote our choice of $\tau = 10^{-3}$ s with a black dashed line. It can be seen that for higher values of τ, the two crossovers happen at frequencies further away from each other, whereas for smaller values of τ, the crossover frequencies converge, until eventually the transition from the Newtonian-fluid behavior to the free membrane limit occurs without an intermediate Maxwell-model regime. The vertical red dotted line denotes the crossover frequency $\omega_{2D}^{\text{elastic}}$ from elastic to viscous interfacial response, as defined in Eq. (29). This line intersects the horizontal black dashed line very closely to the crossover from bulk-dominated Maxwell-model dispersion to free-membrane interface-dominated dispersion, highlighting again that the two crossovers (bulk to interface dominated wave; elastic to viscous in-

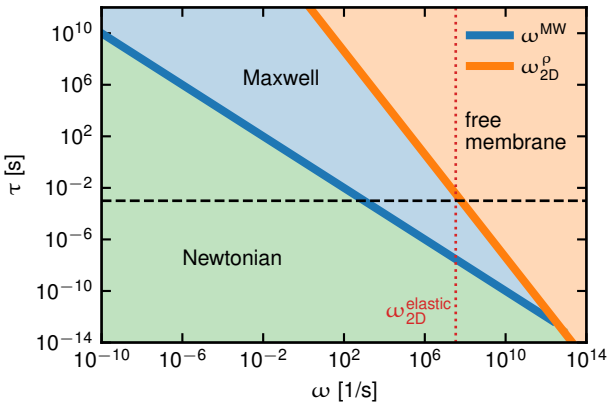

FIG. 4. Phase diagram showing the crossover frequencies found from the analytical solution of the Lucassen wave on the polymer solution-polymer solution interface (55). The crossover from Newtonian to Maxwell-fluid is denoted by ω^{MW} (blue line), whereas the crossover to the free membrane limit is denoted by ω_{2D}^{ρ} (orange line). The red dotted line shows the crossover from elastic to viscous response $\omega_{2D}^{\text{elastic}}$. The black dashed line shows our choice of $\tau = 10^{-3}$ s as an example.

terfacial response) occur simultaneously in Fig. 3 (b), (d).

In summary, we observe that the Lucassen wave at the interface of Maxwell-fluids introduces two new scalings with power-law $k \sim \omega^{1/2}$, which are distinctly different from the corresponding wave solution in the purely viscous case except for the highest frequencies shown. Moreover, the crossover frequency ω^{ρ}_{2D} marking the dominance of the interface properties over bulk properties occurs at a lower frequency than in the corresponding Newtonian-fluid case.

V. CONCLUSIONS

In the present work we derive the general conditional Eq. (12), which governs linear waves at planar viscoelastic interfaces that separate two linear, homogeneous, isotropic viscoelastic bulk materials. We show how viscoelastic Rayleigh waves, and generalizations of capillary-gravity-flexural and Lucassen waves, as well as the equations from elastic plate theory, follow from our general relation. Focussing mainly on the Lucassen wave, we numerically solve the general dispersion relation, and compare the result to analytical limiting cases, for several explicit example systems, including a viscoelastic interface separating two Newtonian fluids, Kelvin-Voigt materials, and Maxwell fluids. For each case we identify and interpret the intermediate power-law scaling regimes of the wave phase velocity and propagation distance.

From a theoretical perspective, our work unifies the derivation of a wide variety of surface waves, and uncovers relations between them. For example, our results make explicit that oscillations of an elastic plate in vacuum are in fact a limiting case of capillary-gravity-flexural waves. Our theory thus enables to systematically study the interrelations and parameter- and frequency-dependent crossovers between different wave solutions. This will in particular serve as a bridge to connect the extensive literature on waves on viscoelastic materials [65–67] to the literature on water wave theory [3, 4, 68].

From a more practical perspective, our results have several applications: Just as viscoelastic Rayleigh waves can be used to measure properties of the material they are excited on [41], or the damping of capillary waves can be used to infer the viscosity of a Newtonian fluid [69], the dispersion relations we derive here can be used to determine mechanical properties of both interface and bulk media, a topic which continues to be of importance in soft matter physics [41, 58, 70, 71]. More explicitly, after experimentally identifying the various power-law scaling regimes of phase velocity and propagation distance of periodically excited Lucassen waves, the analytical viscoelastic Lucassen dispersion relation can be inverted to extract the characteristic viscoelastic timescales of the system under consideration. In particular, the high-frequency properties of viscoelastic surface waves provide a route to probe the non-Newtonian nature of water on short time scales; here, the surface-wave approach can complement established bulk-based experiments [53].

From a biophysical perspective, our theory for Lucassen waves in the presence of viscoelastic bulk media serves as a starting point for investigating the properties of interfacial sound pulses as carriers of information, which has possible relevance for acoustic nerve pulse propagation phenomena [13–15]. Interfaces in biological systems are typically immersed in a hydrogel environment, for which a viscoelastic description is more appropriate than a simple Newtonian fluid model. In this context it will be particularly interesting to understand how bulk viscoelasticity changes the properties of nonlinear sound waves at interfaces, which so far have exclusively been studied for Newtonian bulk fluids [15, 16]. One particularly interesting aspect of the Lucassen wave is the dependence of phase velocities and propagation distances on the membrane compressibility K_{2D}, which according to Eqs. (15), (16), (47), is, for a wave dominated by membrane elasticity and viscous bulk inertia, given by

$$c \sim \sqrt{K_{2D}}\,, \tag{56}$$

$$\beta^{-1} \sim \sqrt{K_{2D}}\,. \tag{57}$$

In our continuum model, modifications in the physical system under consideration are incorporated by changing the model parameters. For example, an axon membrane with a myelin sheath around it can be modeled as an effective interface, with an effective area modulus K_{2D}, assuming that myelin sheath and axon membrane are rigidly connected. Although direct experimental measurements are lacking, it is predicted that a myelin membrane has a larger area modulus K_{2D} as compared to the membrane of an unmyelinated axon [23, 72–74]. We would therefore expect that myelination increases the area modulus of the effective axon interface, which according to Eqs. (56), (57), would then both speed up pressure waves and enhance their propagation distance. As has been noted before in the context of pressure waves in cylinders [23], this acceleration of the pulse is similar to what is observed in saltatory conduction, where myelinated axons lead to action potentials that travel faster, as compared to their unmyelinated counterparts. Similarly, if anesthetics solvated in the lipid membrane indeed decrease the area modulus K_{2D}, as suggested in Ref. [23], the Meyer-Overton rule would be fully consistent with the properties of the Lucassen wave, which according Eqs. (56), (56), leads to slower and more strongly damped waves, and hence less efficient pulse propagation.

A possible extension of this work includes the effects of a time-dependent external force acting on the interface, providing a theory to be used for surface microrheology [39, 40].

Appendix A: Table of parameters

In Tab. I, we summarize all parameters that appear in this paper. The parameters for media I, II and III were

TABLE I. Parameters appearing in our description of the viscoelastic media. For the bulk media parameters, the index $M \in \{\mathrm{I}, \mathrm{III}\}$ labels the medium.

bulk media		
	$\tilde{g}_{M,s}(\omega)$	shear relaxation func.
	$\tilde{g}_{M,d}(\omega)$	dilational relaxation func.
	ρ_M	(volume) mass density
	η_M	shear viscosity
	η'_M	dilational viscosity
	K_M	bulk modulus
	E_M	elastic modulus in Kelvin-Voigt model
	τ_M	stress relaxation time in Maxwell model
	c	speed of sound
	P	pressure
interface		
	$\eta_{2\mathrm{D}}$	in-plane shear viscosity
	$\eta'_{2\mathrm{D}}$	in-plane dilational viscosity
	$\eta^{\perp}_{2\mathrm{D}}$	transversal shear viscosity
	$\kappa_{2\mathrm{D}}$	bending rigidity
	$-\sigma_{2\mathrm{D}}$	2D pressure
	$\rho_{2\mathrm{D}}$	(area) mass density
	$\tilde{g}_{2\mathrm{D}}(\omega)$	in-plane relaxation func.
	$\tilde{\Pi}_{2\mathrm{D}}$	out-of-plane relaxation func.
bulk media & interface		
	g	gravitational acceleration

all introduced in Sec. II.

Appendix B: Derivation of linear system leading to full dispersion relation

A review of the derivation of the continuum mechanical boundary conditions of two bulk media divided by a viscoelastic surface was given by Kralchevsky et. al. [45]. The interface is assumed to have a purely viscous shear response with viscosity $\eta_{2\mathrm{D}}$, a viscoelastic response under dilation with viscosity $\eta'_{2\mathrm{D}}$ and a position-dependent surface tension σ. For out-of-plane deformations, a bending rigidity $\kappa_{2\mathrm{D}}$ and a transverse viscosity $\eta^{\perp}_{2\mathrm{D}}$ is taken into account. Furthermore, the interface has an area mass density $\rho_{2\mathrm{D}}$. In Ref. [22], it is shown that the surface tension of the interface can be written as

$$\sigma_{2\mathrm{D}}(\boldsymbol{r}, t) = \sigma_{2\mathrm{D}} + K_{2\mathrm{D}} \partial_\beta u_\beta \ , \tag{B1}$$

where $\sigma_{2\mathrm{D}}$ is the constant equilibrium surface tension, $K_{2\mathrm{D}}$ is the 2D modulus of compression of the surface, and we use the convention that Greek indices run over $\{x, y\}$, while Latin indices run over $\{x, y, z\}$. Combining Eq. (B1) with the results of Ref. [45], the boundary conditions

$$\begin{aligned}\rho_{2\mathrm{D}} \partial_t^2 u_{2\mathrm{D},\alpha} = &\left(\sigma_{\mathrm{III},z\alpha} - \sigma_{\mathrm{I},z\alpha}\right) \\ &+ \left(K_{2\mathrm{D}} + \eta'_{2\mathrm{D}} \partial_t\right) \partial_\alpha \partial_\beta u_{2\mathrm{D},\beta} \\ &+ \eta_{2\mathrm{D}} \partial_t \partial_\beta^2 u_{2\mathrm{D},\alpha} \ , \qquad \text{for } \alpha \in \{x, y\}\end{aligned} \tag{B2}$$

$$\begin{aligned}\rho_{2\mathrm{D}} \partial_t^2 u_{2\mathrm{D},z} = &\left(\sigma_{\mathrm{III},zz} - \sigma_{\mathrm{I},zz}\right) - \rho_{2\mathrm{D}} g \left(1 - \partial_\beta u_{2\mathrm{D},\beta}\right) \\ &+ \left(\sigma_{2\mathrm{D}} + \eta^{\perp}_{2\mathrm{D}} \partial_t - \kappa_{2\mathrm{D}} \partial_\beta^2\right) \partial_\beta^2 u_{2\mathrm{D},z}\end{aligned} \tag{B3}$$

are derived in Ref. [22]. Here, $\rho_{2\mathrm{D}}$ is the constant equilibrium surface mass density of the interface, $\boldsymbol{u}_{2\mathrm{D}}$ is the displacement of the interface, and all functions of position are understood to be evaluated at $z = 0$.

Including gravitational restoring forces in the boundary condition, the temporal Fourier transform of the stress tensor (2) at the interface $z = 0$ is given by [22]

$$\begin{aligned}\tilde{\sigma}_{jk}(\omega) = &-\delta_{jk} \left[\delta(\omega) P_0 - g \rho \tilde{u}_z(\omega)\right] \\ &+ (-i\omega) \tilde{g}_s(\omega) \tilde{\epsilon}_{jk}(\omega) \\ &+ \delta_{jk} \frac{-i\omega}{3} \left[\tilde{g}_d(\omega) - \tilde{g}_s(\omega)\right] \tilde{\epsilon}_{ll}(\omega) \ ,\end{aligned} \tag{B4}$$

where P_0 is the constant background pressure at $z = 0$ and the displacement field $\boldsymbol{u}$ and its derivatives are understood to be evaluated at $z = 0$. Note that according to the surface gravity approximation [46], the gravitational acceleration of the bulk media only enters in the boundary conditions via Eq. (B4) [22].

The continuity conditions at the interface $z = 0$ are obtained by calculating the displacement field (3) from the harmonic wave ansatz (6), (7) for $z > 0$ and $z < 0$, respectively, and equating them at $z = 0$. This yields the two linear equations

$$\begin{pmatrix} ik & -\lambda_{\mathrm{I},t}^{-1} & -ik & -\lambda_{\mathrm{III},t}^{-1} \\ \lambda_{\mathrm{I},l}^{-1} & ik & \lambda_{\mathrm{III},l}^{-1} & -ik \end{pmatrix} \begin{pmatrix} \Phi_{\mathrm{I}} \\ \Psi_{\mathrm{I}} \\ \Phi_{\mathrm{III}} \\ \Psi_{\mathrm{III}} \end{pmatrix} = \begin{pmatrix} 0 \\ 0 \end{pmatrix} \ , \tag{B5}$$

where $\lambda_{\mathrm{I},l}^{-1}, \lambda_{\mathrm{I},t}^{-1}, \lambda_{\mathrm{III},l}^{-1}, \lambda_{\mathrm{III},t}^{-1}$ are given by Eqs. (8), (9). The stress continuity equations are obtained by calculating $\tilde{\sigma}_{\mathrm{I},ij}$, $\tilde{\sigma}_{\mathrm{III},ij}$ and $\tilde{u}_{2\mathrm{D},i} = \left(\tilde{u}_{\mathrm{I},i}|_{z=0} + \tilde{u}_{\mathrm{III},i}|_{z=0}\right)/2$ for the displacement field Eq. (3), and then substituting the result into Eqs. (B2), (B3). For (B2), only the $\alpha = x$ case is needed, since a short calculation shows that the $\alpha = y$ equation is fulfilled trivially. For the stress tensors of media I, III we use the generalized form (B4) to include effects of gravity [22]. The resulting equations for the stress boundary conditions are

$$\begin{aligned}0 = &\ ik \left[i\omega\rho_{2\mathrm{D}} - k^2 \tilde{g}_{2\mathrm{D}} - 2\tilde{g}_{\mathrm{I},s} \lambda_{\mathrm{I},l}^{-1}\right] \Phi_{\mathrm{I}} \\ &+ \left[\lambda_{\mathrm{I},t}^{-1} \left(-i\omega\rho_{2\mathrm{D}} + k^2 \tilde{g}_{2\mathrm{D}}\right) + \tilde{g}_{\mathrm{I},s}(k^2 + \lambda_{\mathrm{I},t}^{-2})\right] \Psi_{\mathrm{I}} \\ &+ ik \left[i\omega\rho_{2\mathrm{D}} - k^2 \tilde{g}_{2\mathrm{D}} - 2\tilde{g}_{\mathrm{III},s} \lambda_{\mathrm{III},l}^{-1}\right] \Phi_{\mathrm{III}} \\ &+ \Big[- \lambda_{\mathrm{III},t}^{-1} \left(-i\omega\rho_{2\mathrm{D}} + k^2 \tilde{g}_{2\mathrm{D}}\right) \\ &\qquad - \tilde{g}_{\mathrm{III},s}(k^2 + \lambda_{\mathrm{III},t}^{-2})\Big] \Psi_{\mathrm{III}}\end{aligned} \tag{B6}$$

$$
\begin{aligned}
0 = [&\lambda_{\mathrm{I},l}^{-1}\left(\omega^2\rho_{2\mathrm{D}} - k^2\tilde{\Pi}_{2\mathrm{D}} - 2g\rho_{\mathrm{I}}\right) \\
&- k^2\rho_{2\mathrm{D}}g + i\omega\tilde{g}_{\mathrm{I},s}\left(k^2 + \lambda_{\mathrm{I},t}^{-2}\right)]\Phi_{\mathrm{I}} \\
&+ ik[\omega^2\rho_{2\mathrm{D}} - k^2\tilde{\Pi}_{2\mathrm{D}} - 2g\rho_{\mathrm{I}} \\
&+ \lambda_{\mathrm{I},t}^{-1}(2i\omega\tilde{g}_{\mathrm{I},s} - g\rho_{2\mathrm{D}})]\Psi_{\mathrm{I}} \\
&+ [-\lambda_{\mathrm{III},l}^{-1}\left(\omega^2\rho_{2\mathrm{D}} - k^2\tilde{\Pi}_{2\mathrm{D}} + 2g\rho_{\mathrm{III}}\right) \\
&- k^2\rho_{2\mathrm{D}}g - i\omega\tilde{g}_{\mathrm{III},s}\left(k^2 + \lambda_{\mathrm{III},t}^{-2}\right)]\Phi_{\mathrm{III}} \\
&+ ik[\omega^2\rho_{2\mathrm{D}} - k^2\tilde{\Pi}_{2\mathrm{D}} + 2g\rho_{\mathrm{III}} \\
&+ \lambda_{\mathrm{III},t}^{-1}(2i\omega\tilde{g}_{\mathrm{III},s} + g\rho_{2\mathrm{D}})]\Psi_{\mathrm{III}} \ , \qquad \text{(B7)}
\end{aligned}
$$

where again $\lambda_{\mathrm{I},l}^{-1}$, $\lambda_{\mathrm{I},t}^{-1}$, $\lambda_{\mathrm{III},l}^{-1}$ and $\lambda_{\mathrm{III},t}^{-1}$ are given by Eqs. (8), (9), and where $\tilde{g}_{2\mathrm{D}}(\omega)$, $\tilde{\Pi}_{2\mathrm{D}}(k,\omega)$ are defined via Eqs. (13), (14).

The homogeneous linear system of Eqs. (B5), (B6), (B7) for the coefficients Φ_{I}, Ψ_{I}, Φ_{III} and Ψ_{III} has a non-trivial solution if and only if the determinant of the coefficient matrix is zero. Calculating this determinant and equating it with zero, we obtain the conditional Eq. (12).

Appendix C: Rayleigh waves at the fluid-fluid interface

As discussed in Sec. III A, we find a Rayleigh-type surface wave even in the symmetric case, if a planar interface (without any interfacial properties) within an infinitely extended bulk medium is considered.

More explicitly, upon removing the effects related to the surface ($\rho_{2\mathrm{D}} = 0$, $\tilde{g}_{2\mathrm{D}} = 0$, $\tilde{\Pi}_{2\mathrm{D}} = 0$) Eq. (30) becomes Eq. (32), which can also be written as

$$0 = \alpha^4 - k^2\lambda_l^{-1}\lambda_t^{-1} \ . \qquad \text{(C1)}$$

This equation gives rise to two Rayleigh-type wave solutions $k(\omega)$. Note that by setting all interfacial properties equal to zero, we reduce our setup to an infinite space of one bulk fluid, and the existence of the Rayleigh-type wave solutions indicates that a waves of this type can exist along any plane in a bulk fluid.

A plot comparing the two solutions of Eq. (C1) for water and the traditional Rayleigh wave Eq. (35) at the vacuum-water interface is shown in Fig. 5.

Appendix D: Breakdown of Lucassen wave on Kelvin-Voigt interface

As discussed in Sec. IV B 1, at $\omega_{\mathrm{KV}}^{\mathrm{min}} = 2.29/\mathrm{s}$, the numerical Lucassen wave solution of Eq. (30) seizes to exist. In Fig. 6, we show that the real part of $\lambda_t^{-1}(k,\omega)$ approaches zero as ω approaches $\omega_{\mathrm{KV}}^{\mathrm{min}} = 2.29/\mathrm{s}$, so that the transversal decay length diverges; the wave hence seizes to be a surface wave, which rationalizes the breakdown of the Lucassen wave.

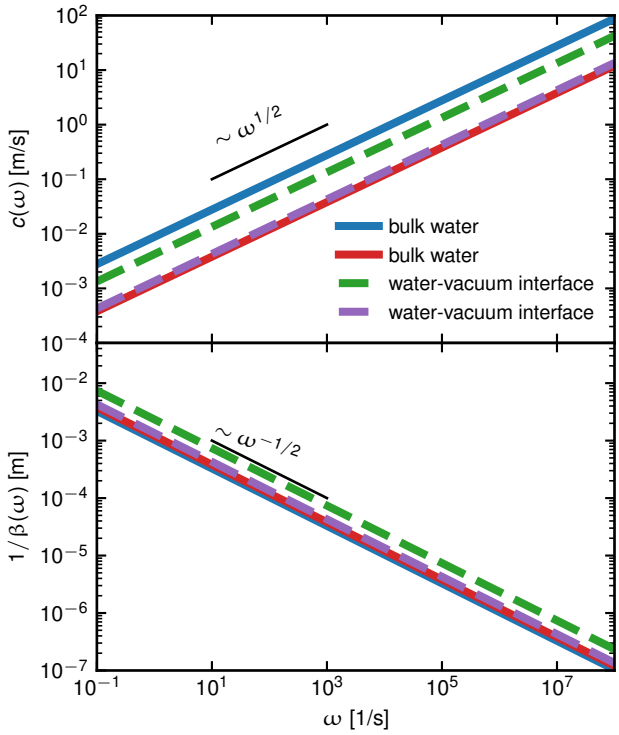

FIG. 5. Rayleigh wave solutions on an arbitrary plane in a body of water (solid) versus the traditional Rayleigh wave solutions at the vacuum-water interface (dashed). The dispersion relations for traditional Rayleigh wave Eq. (35) and for Rayleigh waves at the fluid-fluid interface Eq. (C1) are solved numerically to obtain the wave number k as a function of ω. Phase velocities and propagation distances are obtained from $k(\omega)$ via Eqs. (15), (16).

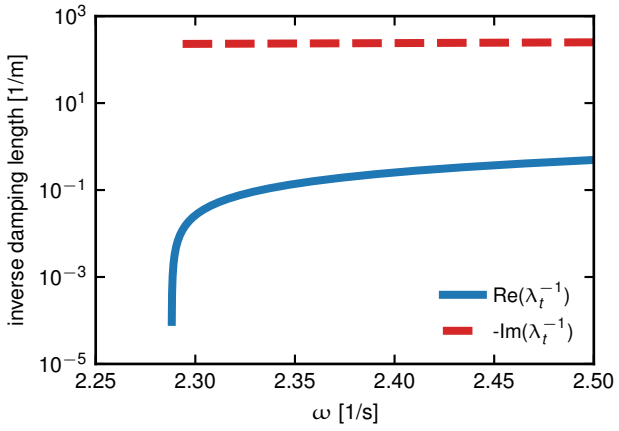

FIG. 6. Plot of real and imaginary parts of the inverse transversal damping length $\lambda_t^{-1}(k,\omega)$ in the frequency region of the breakdown of the Lucassen wave for a purely elastic membrane bounded by half-spaces of polymer gels modelled as Kelvin-Voigt fluids, obtained by inserting the numerical solution $k(\omega)$ of Eq. (30) into Eq. (9). Dashed lines show negative values.

ACKNOWLEDGMENTS

This research has been partially funded by Deutsche Forschungsgemeinschaft (DFG) through grant CRC 1114 "Scaling Cascades in Complex Systems", Project Number 235221301, Project C02 "Interface dynamics: Bridging stochastic and hydrodynamic descriptions".

[1] G. B. Airy, Tides and waves, in *Encyclopaedia Metropolitana (1817-1845), Mixed Sciences*, Vol. 3, edited by H. J. Rose *et al.* (1841).

[2] W. Thomson, Ripples and Waves*, Nature **5**, 1 (1871).

[3] D. J. Acheson, *Elementary fluid dynamics*, Oxford applied mathematics and computing science series (Clarendon, Oxford, 1990).

[4] L. D. Landau, E. M. Lifshits, J. B. Sykes, and W. H. Reid, *Fluid mechanics*, A-W series in advanced physics (Pergamon; Addison-Wesley, Oxford Reading, Mass, 1959).

[5] A. D. D. Craik, The origins of water wave theory, Annual Review of Fluid Mechanics **36**, 1 (2004).

[6] A. D. D. Craik, George Gabriel Stokes on Water Wave Theory, Annual Review of Fluid Mechanics **37**, 23 (2005).

[7] T. Chou, Band structure of surface flexural-gravity waves along periodic interfaces, Journal of Fluid Mechanics **369**, 333 (1998).

[8] F. Monroy and D. Langevin, Direct Experimental Observation of the Crossover from Capillary to Elastic Surface Waves on Soft Gels, Physical Review Letters **81**, 3167 (1998).

[9] M. Van Den Tempel and R. P. Van De Riet, Damping of Waves by Surface-Active Materials, The Journal of Chemical Physics **42**, 2769 (1965).

[10] J. Lucassen, Longitudinal capillary waves. Part 1.–Theory, Transactions of the Faraday Society **64**, 2221 (1968).

[11] J. Lucassen, Longitudinal capillary waves. Part 2.–Experiments, Transactions of the Faraday Society **64**, 2230 (1968).

[12] J. Lucassen and M. Van Den Tempel, Longitudinal waves on visco-elastic surfaces, Journal of Colloid and Interface Science **41**, 491 (1972).

[13] J. Griesbauer, A. Wixforth, and M. F. Schneider, Wave Propagation in Lipid Monolayers, Biophysical Journal **97**, 2710 (2009).

[14] J. Griesbauer, S. Bössinger, A. Wixforth, and M. F. Schneider, Propagation of 2D Pressure Pulses in Lipid Monolayers and Its Possible Implications for Biology, Physical Review Letters **108**, 198103 (2012).

[15] S. Shrivastava and M. F. Schneider, Evidence for two-dimensional solitary sound waves in a lipid controlled interface and its implications for biological signalling, Journal of The Royal Society Interface **11**, 20140098 (2014).

[16] J. Kappler, S. Shrivastava, M. F. Schneider, and R. R. Netz, Nonlinear fractional waves at elastic interfaces, Physical Review Fluids **2**, 114804 (2017), publisher: American Physical Society.

[17] L. Rayleigh, On Waves Propagated along the Plane Surface of an Elastic Solid, Proceedings of the London Mathematical Society **s1-17**, 4 (1885).

[18] P. K. Currie, M. A. Hayes, and P. M. Oleary, Viscoelastic Rayleigh-Waves, Quarterly of Applied Mathematics **35**, 35 (1977).

[19] P. K. Currie and P. M. Oleary, Viscoelastic Rayleigh-Waves II, Quarterly of Applied Mathematics **35**, 445 (1978).

[20] W. Lowrie, *Fundamentals of geophysics*, 2nd ed. (Cambridge University Press, Cambridge, 2007).

[21] G. Hévin, O. Abraham, H. A. Pedersen, and M. Campillo, Characterization of surface cracks with Rayleigh waves: a numerical model, NDT & E International **31**, 289 (1998).

[22] J. Kappler and R. R. Netz, Multiple surface wave solutions on linear viscoelastic media, EPL **112**, 19002 (2015).

[23] M. M. Rvachev, On axoplasmic pressure waves and their possible role in nerve impulse propagation, Biophysical Reviews and Letters **05**, 73 (2010), publisher: World Scientific Publishing Co.

[24] B. Drukarch, H. A. Holland, M. Velichkov, J. J. G. Geurts, P. Voorn, G. Glas, and H. W. de Regt, Thinking about the nerve impulse: A critical analysis of the electricity-centered conception of nerve excitability, Progress in Neurobiology **169**, 172 (2018).

[25] J. Engelbrecht, T. Peets, and K. Tamm, Electromechanical coupling of waves in nerve fibres, Biomechanics and Modeling in Mechanobiology **17**, 1771 (2018).

[26] G. Fongang Achu, F. M. Moukam Kakmeni, and A. M. Dikande, Breathing pulses in the damped-soliton model for nerves, Physical Review E **97**, 012211 (2018), publisher: American Physical Society.

[27] L. Holland, H. W. de Regt, and B. Drukarch, Thinking About the Nerve Impulse: The Prospects for the Development of a Comprehensive Account of Nerve Impulse Propagation, Frontiers in Cellular Neuroscience **13**, 10.3389/fncel.2019.00208 (2019), publisher: Frontiers.

[28] H. Barz, A. Schreiber, and U. Barz, Nerve impulse propagation: Mechanical wave model and HH model, Medical Hypotheses **137**, 109540 (2020).

[29] M. Mussel and M. F. Schneider, Sound pulses in lipid membranes and their potential function in biology, Progress in Biophysics and Molecular Biology 10.1016/j.pbiomolbio.2020.08.001 (2020).

[30] H. Meyer, Zur Theorie der Alkoholnarkose, Archiv für experimentelle Pathologie und Pharmakologie **42**, 109 (1899).

[31] C. E. Overton, *Studien über die Narkose zugleich ein Beitrag zur allgemeinen Pharmakologie* (G. Fischer, Jena, 1901).

[32] I. Tasaki and P. M. Byrne, Heat Production Associated with a Propagated Impulse in Bullfrog Myelinated Nerve Fibers, The Japanese Journal of Physiology **42**, 805 (1992).

[33] G. H. Kim, P. Kosterin, A. L. Obaid, and B. M. Salzberg, A Mechanical Spike Accompanies the Action Potential in Mammalian Nerve Terminals, Biophysical Journal **92**, 3122 (2007).

[34] A. El Hady and B. B. Machta, Mechanical surface waves accompany action potential propagation, Nature Communications **6**, 6697 (2015).

[35] J. L. Harden and H. Pleiner, Hydrodynamic modes of viscoelastic polymer films, Physical Review E **49**, 1411 (1994).

[36] A. J. Levine and F. C. MacKintosh, Dynamics of viscoelastic membranes, Physical Review E **66**, 061606 (2002).

[37] G. K. Rajan and D. M. Henderson, Linear waves at a surfactant-contaminated interface separating two fluids: Dispersion and dissipation of capillary-gravity waves, Physics of Fluids **30**, 072104 (2018).

[38] G. K. Rajan, Dissipation of interfacial Marangoni waves and their resonance with capillary-gravity waves, International Journal of Engineering Science **154**, 103340 (2020).

[39] Y. Onodera and P.-K. Choi, Surface-wave modes on soft gels, The Journal of the Acoustical Society of America **104**, 3358 (1998).

[40] C. Bar-Haim and H. Diamant, Surface Response of a Polymer Network: Semi-infinite Network, Langmuir **36**, 3981 (2020), publisher: American Chemical Society.

[41] X. Shao, J. R. Saylor, and J. B. Bostwick, Extracting the surface tension of soft gels from elastocapillary wave behavior, Soft Matter **14**, 7347 (2018), publisher: The Royal Society of Chemistry.

[42] P. Chantelot, L. Domino, and A. Eddi, How capillarity affects the propagation of elastic waves in soft gels, Physical Review E **101**, 032609 (2020), publisher: American Physical Society.

[43] L. D. Landau, E. M. Lifshitŝ, A. M. Kosevich, and L. P. Pitaevskiĭ, *Theory of elasticity*, 3rd ed., Course of theoretical physics (Butterworth-Heinemann, Oxford, 1986).

[44] R. M. Christensen, *Theory of Viscoelasticity*, 2nd ed. (Academic Press, New York, 1982).

[45] P. A. Kralchevsky, J. C. Eriksson, and S. Ljunggren, Theory of curved interfaces and membranes: Mechanical and thermodynamical approaches, Advances in Colloid and Interface Science **48**, 19 (1994).

[46] P. Segall, *Earthquake and volcano deformation* (Princeton University Press, Princeton, 2010).

[47] If either λ_l^{-2} or λ_t^{-2} is purely real and negative, both square roots have vanishing real part, but we do not accept such solutions: The wave would not be damped away from the interface.

[48] E. H. Lucassen-Reynders and J. Lucassen, Properties of capillary waves, Advances in Colloid and Interface Science **2**, 347 (1970).

[49] J. C. Earnshaw and E. McCoo, Mode mixing of liquid surface waves, Physical Review Letters **72**, 84 (1994).

[50] A. Mielke, R. R. Netz, and S. Zendehroud, A rigorous derivation and energetics of a wave equation with fractional damping, Journal of Evolution Equations 10.1007/s00028-021-00686-2 (2021).

[51] Sir H. Lamb, *Hydrodynamics*, sixth ed. (Cambridge University Press, 1975).

[52] I. Omelyan, I. Mryglod, and M. Tokarchuk, Wavevector- and frequency-dependent shear viscosity of water: the modified collective mode approach and molecular dynamics calculations, Condensed Matter Physics **8**, 25 (2005).

[53] M. Pelton, D. Chakraborty, E. Malachosky, P. Guyot-Sionnest, and J. E. Sader, Viscoelastic Flows in Simple Liquids Generated by Vibrating Nanostructures, Physical Review Letters **111**, 244502 (2013).

[54] T. J. O'Sullivan, S. K. Kannam, D. Chakraborty, B. D. Todd, and J. E. Sader, Viscoelasticity of liquid water investigated using molecular dynamics simulations, Physical Review Fluids **4**, 10.1103/PhysRevFluids.4.123302 (2019).

[55] J. C. F. Schulz, A. Schlaich, M. Heyden, R. R. Netz, and J. Kappler, Molecular interpretation of the non-Newtonian viscoelastic behavior of liquid water at high frequencies, Phys. Rev. Fluids **5**, 103301 (2020).

[56] R. E. Bolz and G. L. Tuve, *CRC Handbook of Tables for Applied Engineering Science*, 2nd ed. (CRC Press, 2019).

[57] J. Krägel, J. B. Li, R. Miller, M. Bree, G. Kretzschmar, and H. Möhwald, Surface viscoelasticity of phospholipid monolayers at the air/water interface, Colloid and Polymer Science **274**, 1183 (1996).

[58] E. P. Petrov, R. Petrosyan, and P. Schwille, Translational and rotational diffusion of micrometer-sized solid domains in lipid membranes, Soft Matter **8**, 7552 (2012).

[59] E. P. Petrov and P. Schwille, Translational Diffusion in Lipid Membranes beyond the Saffman-Delbrück Approximation, Biophysical Journal **94**, L41–L43 (2008).

[60] C.-H. Lee, W.-C. Lin, and J. Wang, All-optical measurements of the bending rigidity of lipid-vesicle membranes across structural phase transitions, Physical Review E **64**, 020901 (2001).

[61] N. Delorme and A. Fery, Direct method to study membrane rigidity of small vesicles based on atomic force microscope force spectroscopy, Physical Review E **74**, 030901 (2006).

[62] A. Schlaich, J. Kappler, and R. R. Netz, Hydration Friction in Nanoconfinement: From Bulk via Interfacial to Dry Friction, Nano Letters **17**, 5969 (2017).

[63] J. L. Harden, H. Pleiner, and P. A. Pincus, Hydrodynamic surface modes on concentrated polymer solutions and gels, The Journal of Chemical Physics **94**, 5208 (1991).

[64] T. Hiraiwa and R. R. Netz, Systematic bottom-up theory for the viscoelastic response of worm-like chain networks, EPL (Europhysics Letters) **123**, 58002 (2018).

[65] J. M. Carcione, *Wave Fields in Real Media: Wave Propagation in Anisotropic, Anelastic, Porous and Electromagnetic Media*, 2nd ed., Handbook of Geophysical Exploration: Seismic Exploration (Elsevier Science, Amsterdam; Oxford, 2007).

[66] I. A. Viktorov, *Rayleigh and Lamb waves: physical theory and applications*, Ultrasonic technology (Plenum Press, New York, 1967).

[67] R. D. Borcherdt, *Viscoelastic waves in layered media* (Cambridge University Press, Cambridge, 2009).

[68] U. Seifert and S. A. Langer, Viscous Modes of Fluid Bilayer Membranes, Europhysics Letters (EPL) **23**, 71 (1993).

[69] F. Behroozi, J. Smith, and W. Even, Stokes' dream: Measurement of fluid viscosity from the attenuation of capillary waves, American Journal of Physics **78**, 1165 (2010).

[70] G. Espinosa, I. López-Montero, F. Monroy, and D. Langevin, Shear rheology of lipid monolayers and insights on membrane fluidity, Proceedings of the National Academy of Sciences **108**, 6008 (2011).

[71] A. D. Dinsmore, M. F. Hsu, M. G. Nikolaides, M. Marquez, A. R. Bausch, and D. A. Weitz, Colloidosomes: Selectively Permeable Capsules Composed of Colloidal Particles, Science **298**, 1006 (2002).

[72] D. Needham, Cohesion and Permeability of Lipid Bilayer Vesicles, in *Permeability and Stability of Lipid Bilayers*, edited by E. A. Disalvo and S. A. Simon (CRC Press,

1995) Chap. 3, pp. 49–76.
[73] T. E. Thompson, M. B. Sankaram, and C. Huang, Organization and Dynamics of the Lipid Components of Biological Membranes, in *Comprehensive Physiology* (American Cancer Society, 2011) pp. 23–57.
[74] M. Saeedimasine, A. Montanino, S. Kleiven, and A. Villa, Role of lipid composition on the structural and mechanical features of axonal membranes: a molecular simulation study, Scientific Reports **9**, 8000 (2019).